OVO Positively Regulates Essential Maternal Pathways by Binding Near the Transcriptional Start Sites in the *Drosophila* Female Germline

Leif Benner[1,2], Savannah Muron[1], Jillian G. Gomez[1], Brian Oliver[1]

1. Section of Developmental Genomics, Laboratory of Biochemistry and Genetics, National Institute of Diabetes and Digestive and Kidney Diseases, National Institutes of Health, Bethesda, MD, USA.

2. Department of Biology, Johns Hopkins University, Baltimore, MD, USA.

Abstract

Differentiation of female germline stem cells into a mature oocyte includes the expression of RNAs and proteins that drive early embryonic development in *Drosophila*. We have little insight into what activates the expression of these maternal factors. One candidate is the zinc-finger protein OVO. OVO is required for female germline viability and has been shown to positively regulate its own expression, as well as a downstream target, *ovarian tumor*, by binding to the transcriptional start site (TSS). To find additional OVO targets in the female germline and further elucidate OVO's role in oocyte development, we performed ChIP-seq to determine genome-wide OVO occupancy, as well as RNA-seq comparing hypomorphic and wild type rescue *ovo* alleles. OVO preferentially binds in close proximity to target TSSs genome-wide, is associated with open chromatin, transcriptionally active histone marks, and OVO-dependent expression. Motif enrichment analysis on OVO ChIP peaks identified a 5`-TAACNGT-3` OVO DNA binding motif spatially enriched near TSSs. However, the OVO DNA binding motif does not exhibit precise motif spacing relative to the TSS characteristic of RNA Polymerase II complex binding core promoter elements. Integrated genomics analysis showed that 525 genes that are bound and increase in expression downstream of OVO are known to be essential maternally expressed genes. These include genes involved in anterior/posterior/germ plasm specification (*bcd, exu, swa, osk, nos, aub, pgc, gcl*), egg activation (*png, plu, gnu, wisp, C(3)g, mtrm*), translational regulation (*cup*, *orb*, *bru1, me31B*), and vitelline membrane formation (*fs(1)N*, *fs(1)M3*, *clos*). This suggests that OVO is a master transcriptional regulator of oocyte development and is responsible for the expression of structural components of the egg as well as maternally provided RNAs that are required for early embryonic development.

Introduction

Drosophila early embryonic development is directed by events that take place during oogenesis. Germline stem cells (GSCs) asymmetrically divide to renew the stem cell population and send one daughter cell towards oogenesis. In the germarium, oogenesis is preceded by four rounds of incomplete mitotic divisions resulting in a 16-cell egg chamber. One cell is specified as the oocyte which is arrested in prophase of meiosis I, while the rest of the 15 cells enter endoreplication cycles and become nurse cells (NCs). Once the 16 cell egg chamber buds from the germarium, the NCs begin to transcribe and translate a vast array of RNAs and proteins that serve diverse functional roles (Bastock and St Johnston 2008; Spradling et al. 2022). These roles include positioning maternal mRNAs and proteins in the correct spatial orientation to support anterior/posterior, and dorsal ventral axis specification, as well negative regulators of translation to ensure that the maternal mRNAs are not translated before fertilization (Lasko 2012). The oocyte also contains a number of proteins and mRNAs that are needed for egg activation, completion of meiosis and initiation of embryonic development after fertilization (Avilés-Pagán and Orr-Weaver 2018). To repeat the process of oogenesis from generation to generation, germ cells in the developing embryo need to be specified and maintained separately from the rest of the developing somatic cell population. This requires maternally controlled localization of the germ plasm and early pole cell formation in the embryo (Mahowald 2001). While the complex interactions between maternally supplied mRNAs and proteins have been well studied, transcriptional regulation driving the expression of these pathways are less well understood.

Few positive regulators of female specific germ cell transcription have been identified. Genes such as *grauzone* (*grau*) and *maternal gene required for meiosis* (*mamo*) have been shown to activate the transcription of *cortex* and *vasa*, respectively, in the female germline (Harms et al. 2000; S. Nakamura et al. 2019). Active repression of male specific transcription through the activity of *egg*, *wde*, and *Su(var)205* (Smolko, Shapiro-Kulnane, and Salz 2018), or global repression of non-ovarian transcriptional networks

through the function of *sov* (Benner et al. 2019), have shown the importance of heterochromatin formation in the female germline for cellular identity and oocyte development. In fact, recent work has shown the importance of transcriptional repression, mediated through changes in histone modifications, as a key regulator of egg chamber differentiation. GSCs have been shown to exist in a sort of 'ground state' of histone modifications. Characterized with modest non-canonical repressive H3K9me3 and H3K27me3 histone marks at many genes, as well as transcriptionally active H3K27ac histone marks and open chromatin at others (Pang et al. 2023; DeLuca et al. 2020). As oocyte development continues, repressive histone marks associated with heterochromatin begin to increase in abundance resulting in fewer histone marks associated with transcription and open chromatin. This suggests that gene expression becomes more restricted throughout the differentiation process. However, it is unlikely that the female germline directs oocyte development solely through a repressive transcriptional model. Whether the female germline expresses paralogs of the RNA polymerase II complex, like the male germline (M. Hiller et al. 2004; M. A. Hiller et al. 2001; Lu et al. 2020), or if there are pioneering transcription factors involved in determining the open chromatin status for female germ cell-specific expression, or something else entirely, has yet to be determined.

Although few female specific germline transcription factors have been identified, the conserved zinc-finger transcription factor OVO has long been known to be required for female germ cell viability. Female germ cells that are *ovo*$^{-}$ do not survive into adulthood (Oliver, Perrimon, and Mahowald 1987; Oliver, Pauli, and Mahowald 1990; Benner et al. 2023). Hypomorphic *ovo* alleles, specifically ones that disrupt the transcriptional activator OVO-B, show an arrested egg chamber phenotype, indicating that wild-type OVO-B activity is required for oocyte maturation (Salles et al. 2002; Benner et al. 2023). Germline OVO is expressed at all stages of oogenesis, where it is eventually maternally loaded into the egg. Maternal OVO becomes specifically localized to the developing germline and persists throughout embryogenesis until zygotic OVO is expressed (Hayashi et al. 2017; Benner et al. 2023). Thus, OVO is eternally expressed in the female germline, suggesting it may be a key regulator of female specific germline transcription. However, only two downstream targets have previously been identified for OVO. OVO has been shown to positively regulate the expression of its own transcription, therefore executing an autoregulatory loop, as well as positively regulating the transcription of the gene *ovarian tumor* (*otu*)(Lü et al. 1998; Bielinska et al. 2005; Lü and Oliver 2001; Andrews et al. 2000). *otu* is also required in the female germline, where *otu*$^{-}$ germ cells show viability and germline tumor phenotypes (Bishop and King 1984). The *ovo* phenotype is epistatic to that of *otu*, and ectopic *otu* expression cannot rescue female germ cell death due to loss of *ovo* (Hinson, Pettus, and Nagoshi 1999; Pauli, Oliver, and Mahowald 1993). Therefore, *ovo* must be responsible for activating the transcription of genes in addition to *otu* for female germ cell survival and differentiation.

We expanded our knowledge of OVO's role in the female germline by determining genome-wide OVO occupancy and global transcriptional changes downstream of OVO. This allowed us to determine which genes OVO binds, and which genes transcriptionally respond to OVO *in vivo*. We show that OVO is directly regulating essential maternal pathways such as axis specification, primordial germ cell formation, egg activation, and maternal mRNA translation regulation. Together, we show that OVO plays a pivotal role in the positive transcriptional regulation of oocyte and early embryonic development. We show that OVO likely carries out this regulation by binding at or in close proximity to the promoters of the genes it regulates and that OVO DNA binding motifs are enriched at or near the transcriptional start site (TSS) of OVO responsive genes, although the spacing of OVO binding sites suggests that it is not a component of the RNA Polymerase complex. OVO binding is also a signature of open chromatin status and active transcription throughout oocyte differentiation. Altogether, we suggest that OVO is required for the activity of a large number of female germline promoters and is likely a key regulator of oocyte maturation and RNAs and proteins that are required for early embryonic development.

Results

OVO Binds Promoters Genome-Wide

OVO-B, the predominant protein isoform expressed from the *ovo* locus in the female germline (Benner et al. 2023), is a positive regulator of transcription (Andrews et al. 2000) at both the *otu* and *ovo* locus. Transgenic reporter constructs of *otu* and *ovo* require OVO binding sites both at and upstream of the TSS in order to recapitulate full reporter expression (Bielinska et al. 2005; Lü et al. 1998; Lü and Oliver 2001).

Females hemizygous for antimorphic dominant gain-of-function (*ovo*^{D}) or homozygous recessive (*ovo*^{D1rv}) *ovo* alleles lack germ cells in the adult ovary (Oliver, Perrimon, and Mahowald 1987; Benner et al. 2023). True OVO-B null alleles created by deletion of the *ovo-B* promoter have the same germ cell loss phenotype (Benner et al. 2023). The phenotypes of *otu* females range from germ cell death to ovarian tumors depending on the allele and undefined stochastic factors (Bishop and King 1984). It is possible that the germ cell death phenotype in *ovo*$^{-}$ female germ cells can solely be explained by failure of OVO to activate *otu* expression, however, this is highly unlikely. The *ovo*^{D1rv} phenotype is epistatic to *otu*$^{-}$, and ectopic *otu*$^{+}$ expression in *ovo*$^{-}$ germ cells does not rescue the germ cell death phenotype (Hinson, Pettus, and Nagoshi 1999). This suggests that OVO regulates the expression of additional genes in the female germline.

We wanted to identify OVO target genes in the female germline by using two complementary genome-wide approaches to test for OVO presence and function. Specifically, we determined OVO occupancy genome-wide with ChIP-seq, and determined *ovo* function by comparing the RNA expression profiles between *ovo*$^{+}$ and *ovo* hypomorphs in the female germline. In order to determine OVO occupancy genome-wide, we performed ChIP-seq on adult ovaries in triplicate, using two C-terminally tagged alleles as affinity purification tools (*ovo*$^{Cterm\text{-}3xFHA}$ i.e. OVO-HA and *ovo*$^{Cterm\text{-}GFP}$ i.e. OVO-GFP, Figure 1A-C, Figure S1A) (Benner et al. 2023) and called significantly enriched peaks from OVO-HA and OVO-GFP compared to their respective input controls.

We first compared the pulldown results with the OVO-HA versus OVO-GFP ChIP reagents. The GFP pull down appeared to be more efficient, but never-the-less we found excellent agreement, as most OVO-HA peaks were also found in the OVO-GFP dataset. The OVO-GFP ChIP dataset had 7,235 significant ChIP peaks according to peak enrichment analysis genome-wide, while OVO-HA ChIP dataset had 3,393 significant peaks genome-wide (Table S1). To determine the similarity in significant peak calling between the two datasets, we calculated a Jaccard index (intersection/union) between the significantly enriched peaks from the tagged *ovo* allele bearing ovaries. The Jaccard index between OVO-HA and OVO-GFP ChIP peaks was 0.64 (where 0 = no overlap and 1 = full overlap) with a total of 3,094 ChIP peaks overlapping. Thus, almost all significant OVO-HA ChIP peaks were also found within the OVO-GFP ChIP dataset (91% of OVO-HA peaks overlapped OVO-GFP peaks). OVO-GFP pulldown was either more effective, or less likely, promiscuous. Regardless, we decided to use the conservative intersection of the two datasets (3,094 peaks) for downstream OVO occupancy informatics (Table S2).

OVO is a sequence-specific DNA-binding protein, but many transcription factors also have a more general affinity for DNA. Additionally, immunoprecipitation can capture indirect interactions due to nuclear topology in addition to direct sequence-specific binding. For example, in the particular case of OVO TSS binding, this could be direct, as shown in the case of *ovo* and *otu* loci (Lü et al. 1998; Lü and Oliver 2001; Bielinska et al. 2005), or could be due to looping of an OVO-bound enhancer to the core promoter. Determining if there are canonical OVO binding sites at peaks can help to distinguish direct and indirect binding. If OVO is directly binding to the TSS, we would expect to find OVO binding site enrichment at that location. To examine the sequences enriched in peaks, we looked directly for the known OVO binding sites previously defined by footprinting (Lü et al. 1998) and SELEX-seq (Bielinska et al. 2005; Lee and Garfinkel 2000). We also did *de novo* motif finding on this substantial dataset to refine the sequence specific motifs bound by OVO and perhaps other motifs associated with other transcription factors preferentially bound by OVO enhancers, or OVO proximal sites in 3D nuclear space. We performed novel motif enrichment analysis using STREME (Bailey 2021) with our overlapping ChIP peaks and found a number of significant motifs within our dataset. The most significant motif, 5`-TAACGGTAAA-3`, was found in 49% of significant OVO ChIP peaks (Figure 1D, 'Motif One'). This motif is highly similar to the OVO DNA binding motif that has been reported twice before, 5`-AGTAACNGT-3` (SELEX method, 'Garfinkel OVO Motif') and 5`-TGTAACNGT-3` (Footprinting method, 'Oliver OVO Motif'). The only differences between motif one in our dataset and the literature, is that the *de novo* motif is two nucleotides shorter than the previously described motifs at the 5` end, extends 3 nucleotides downstream, and includes a second G near the 3'-end (Figure S1B). Collectively, this is strong evidence that the core OVO binding sequence is 5`-TAACNGT-3`. Some binding sites can be recognized by multiple transcription factors. To determine if other characterized transcription factors recognize this sequence, we searched for significant matches to motif one in the Jaspar database (Castro-Mondragon et

al. 2022) of known *Drosophila* motifs using Tomtom (Gupta et al. 2007). The OVO DNA binding motif ('Garfinkel OVO Motif') was scored as a significant match (Figure S1B, $p<0.05$). Along with the OVO DNA binding motif, other motifs were also significantly enriched in OVO ChIP peaks. The motif 5'-GWGMGAGMGAGABRG-3' (Figure S1C) was found in 18% of OVO ChIP peaks and is a significant match to the DNA binding motifs of the transcription factors GAF (*Trl*) (Omelina et al. 2011) and CLAMP (Soruco et al. 2013). *Trl* germline clones are not viable, indicating that GAF activity is required in the germline during oogenesis (Chen et al. 2009). The possibility that OVO binds with and regulates genes alongside of GAF given the enrichment of both transcription factors DNA binding motifs is intriguing. Other significantly enriched motifs 5'-ACACACACACACACA-3' (29% of peaks, Figure S1D), 5'-RCAACAACAACAACA-3' (26% of peaks, Figure S1E), and 5'-GAAGAAGAAGAAGAR-3' (17% of peaks, Figure S1F) were present in OVO ChIP peaks, however, these motifs did not significantly match known DNA binding motifs of other transcription factors. Determining the factors that bind to these sequences will certainly help elucidate our understanding of transcriptional control with relationship to OVO in the female germline.

Not every peak region had one of the consensus OVO DNA binding motifs. This does not mean *a priori* that they bound OVO indirectly. Motif enrichment can be driven by a few strongly enriched sequences, so that more minor enrichments of variants are missed. Therefore, we carefully examined the 51% of our overlapping OVO ChIP peaks where OVO DNA binding motif one was not found. This second round of *de novo* analysis revealed enrichment of OVO DNA binding motif derivatives. For example, the third most significant motif (found in 37% of peaks) was 5`-RWMTAACGGV-3` (Figure 1E, motif two). This motif had the core 5`-TAACNGT-3` sequence found in all three aforementioned methods, however, the last nucleotide in the core sequence is unspecific and lacks the three 3` nucleotides found in motif one. Two other derivative motifs, 5'-TAACTGTTTT-3' (found in 17% of sequences, Figure 1F, motif three), and 5'-TTACSGTAA-3' (found in 5% of sequences, Figure 1G, motif four), vary within the central core motif (at positions 5 and 2 of the core sequence, respectively) and upstream and downstream ends. Searching for all variations of the OVO DNA binding motif (Table S3) within our significant overlapping ChIP peaks indicated that 72% of peaks contained at least one variation of these four binding motifs. It is a reasonable hypothesis that OVO peaks are most often due to direct, rather than indirect OVO binding.

A prediction for direct OVO binding to motifs, is that the motif should be centered within the peak of fragmented input DNA sequences. Therefore, we plotted the significant ChIP (minus input) read density centered on the location of the motif. We found that the read density for all ChIP peaks that contain each one of the *de novo* OVO motifs, as well as the *in vitro* OVO motifs, are centered over the motif location (Figure 1H). This suggests that all of these motifs from our analysis are bonafide OVO DNA binding sites *in vivo*. While it is possible that OVO comes into contact with regions of DNA in three-dimensional nuclear space non-specifically, the presence of OVO motifs within a large percentage of significant ChIP peaks *in vivo* and enrichment of OVO ChIP read density at the location of the motifs, strongly reinforces the idea that our OVO ChIP dataset contains regions centered on sequences specifically bound by OVO in the ovary.

Given the clear function of OVO occupancy near the TSS of its two known targets, *ovo* and *otu* (Lü et al. 1998; Bielinska et al. 2005; Lü and Oliver 2001), we were interested in determining if OVO peaks are generally near the TSS of other target genes as well. In addition to informing the biology of OVO function, this simplifies the problem of associating peaks to potential functional target genes. As a preliminary test of this idea, we determined if the fully overlapping OVO-HA and OVO-GFP peaks were spatially enriched with respect to the currently annotated gene model elements such as TSS, open reading frames (ORFs), or transcription termination sequences (TTS). If the TSS association of OVO at the two known targets reflects a general propensity, then we expect OVO ChIP peaks to be more closely associated with TSS than other gene elements. To carry out this analysis, we normalized the genome for these three gene elements, such that the distance between adjacent loci was 1. If there is no enrichment for OVO peaks to a specific gene element, then the peak location would have an equal frequency from 0.0 to 0.5 relative distance. Measuring the relative distance of our OVO ChIP peaks to TSS, ORFs, and TTS, showed that the OVO binding was highly enriched near TSS/promoter locations and was not correlated with ORF and TTS locations (Figure 1I). These results confirmed that OVO is characterized by core promoter proximal binding. Since OVO ChIP peaks as a class are associated with TSS, we plotted the ChIP minus input

read density of genes that overlap significant ChIP peaks to examine the full distribution. We found that the OVO ChIP read density was highly enriched over the TSS and was not due to a few highly enriched examples (Figure 1J). This builds on the idea that OVO is binding directly over, or in close proximity to the TSS of its target genes genome-wide. In other words, the previous work showing OVO binding the *ovo-B* and *otu* TSS (Bielinska et al. 2005; Lü et al. 1998; Lü and Oliver 2001) is typical. This very specific binding of OVO to the TSS is intriguing and unusual, as this region associates with the basal transcriptional machinery. It raises the possibility that OVO is not a typical transcription factor that acts primarily via enhancer binding but might be part of the core promoter binding complex or acts to precondition the core promoter region for example.

Although OVO ChIP peaks overlapping genes showed a strong read density enrichment over the TSS, we found that only 45% (1,394/3,094) of OVO ChIP peaks directly overlapped a TSS. 43% (1,339/3,094) of OVO ChIP peaks were found to overlap the gene body downstream of the TSS (intronic and exonic sequences) and 12% (366/3,094) did not overlap any gene elements, indicating that they were intergenic. We were interested in the differences between OVO binding directly over the TSS or at more distal upstream and downstream sites. We decided to plot the OVO ChIP read density of these different classes of OVO binding patterns and found that OVO bound over the TSS produced a sharp read density enrichment over the TSS which was consistent with what was found for all OVO bound genes (Figure 1K). OVO binding along the gene body surprisingly also showed a read density enrichment over the TSS, although the magnitude of read density enrichment was notably less than TSS OVO binding. Intergenic OVO binding also showed these same characteristics with a notable upstream read density enrichment possibly indicative of enhancer binding. This indicates that although the significantly called OVO ChIP peaks did not overlap the TSS, there was still a propensity for TSS sequences to be enriched with OVO ChIP over the input control. This could be due to weaker direct *in vivo* binding of OVO to these TSSs or indirect interactions between the upstream/downstream OVO bound sequences and the TSS, possibly through a looping enhancer-promoter interaction. However, regardless of the location of the OVO ChIP peak, OVO seemed to always be enriched at or in close proximity to TSSs.

The OVO ChIP read density was highly enriched over the annotated TSS of target genes, but TSS annotation is challenging and can be tissue specific. We were interested in empirically determining if the same enrichment was present in TSSs utilized specifically in ovarian tissue. The 5' ends of mRNA are capped. In order to determine where these caps mapped to the genome, we analyzed Cap Analysis of Gene Expression (CAGE-seq) data from adult *Drosophila* ovaries (Chen et al. 2014) and extracted the dominant significant TSSs in the ovary. CAGEr predicted 6,856 significant TSSs in the ovary dataset, of which 1,047 overlapped with OVO ChIP peaks. We plotted the OVO ChIP minus input read density centered on the significant ovary CAGE-seq TSSs for TSSs that overlapped or did not overlap OVO ChIP peaks (Figure 1L). We found that OVO ChIP read density was highly enriched over the location of TSSs from ovary CAGE-seq that overlapped OVO ChIP peaks when compared to TSSs that did not overlap OVO ChIP peaks. Thus, OVO TSS binding is not due to poor annotation of ovarian TTSs. Furthermore, OVO is binding at or near TSSs of genes actively being transcribed in the ovary.

<u>OVO Binding is Associated with Open Chromatin and Transcriptionally Active Histone Marks</u>

Our OVO ChIP data indicated that OVO was binding at or in close proximity to promoters genome-wide. OVO could have a positive and/or negative effect on transcription at these locations. For example, OVO could help recruit or sterically hinder RNA Polymerase binding to TSSs. However, previous *ovo* reporter constructs show positive effects of OVO binding near TSS (Lü and Oliver 2001; Lü et al. 1998; Bielinska et al. 2005). If OVO binding is generally promoting transcription, then we hypothesize that it would be more closely associated with histone marks associated with active transcription, such as H3K27ac and H3K4me3, as well as lower nucleosome density that can be measured through ATAC-seq. In contrast, OVO binding would be expected to negatively correlate with repressive H3K9me3 and H3K27me3 histone marks and higher nucleosome density. It is technically difficult to determine changes in chromatin status and transcription in germ cells that lack OVO, as the phenotype is cell death (although we will return to this later for transcription profiling) but analyzing OVO binding in the context of ovarian chromatin was highly informative.

Recent work profiling nucleosome density and histone marks have shown that female GSCs have a 'ground state' chromatin profile (DeLuca et al. 2020), similar to the histone mark profiles that are found in early embryos (Li et al. 2014). This has been characterized to contain non-canonical H3K27me3 profiles and low H3K9me3 histone levels (Pang et al. 2023; DeLuca et al. 2020). As egg follicles differentiate, nurse cells begin to accumulate H3K9me3 marks, and H3K27me3 histone marks begin to accumulate over more traditional polycomb domains. This in turn leads to a decrease in the number of open chromatin peaks as well as H3K27ac histone marks, which are generally associated with active transcription (Pang et al. 2023; DeLuca et al. 2020). Essentially, these data support the idea that egg chambers restrict gene expression competency as they differentiate.

In order to determine the relationship in our OVO ChIP data and other chromatin marks, we analyzed GSC H3K27ac, H3K27me3, H3K9me3, H3K4me3, and ATAC-seq data (Pang et al. 2023; DeLuca et al. 2020) with the same parameters used to establish significant OVO peaks in our OVO ChIP dataset. Our OVO ChIP data was from one day old ovaries, and we did not profile specific follicle stages. So we also analyzed 32c (roughly stage 5 egg chambers) H3K27ac, H3K27me3, ATAC-seq, and 8c H3K9me3 (32c was not available) histone marks (Pang et al. 2023; DeLuca et al. 2020) to see if there were any stage specific differences in comparison to OVO DNA binding. We focused specifically on GSC and 32c egg follicles for these chromatin marks since that is when the *ovo* hypomorphic egg chambers arrest (Benner et al. 2023). We first plotted the read density of each respective chromatin mark minus their input control centered on either the OVO ChIP peak local maximum (Figure 2A) or OVO DNA binding motifs contained within significant OVO ChIP peaks (Figure 2B). GSC ATAC and H3K27ac read density showed a high degree of enrichment over OVO ChIP peak maximums (Figure 2A) and OVO DNA binding motifs (Figure 2B), consistent with positive transcriptional activity. GSC H3K4me3 read density was, to a lesser extent, also enriched with OVO ChIP peak maximums and OVO DNA binding motifs. However, there was no read density enrichment for repressive GSC H3K27me3 and H3K9me3 histone marks. The same findings generally held true when looking at the overlap of OVO ChIP peaks and chromatin marks in differentiating egg chambers. Notably, there was an even higher read density enrichment over OVO ChIP peak maximum and DNA binding motifs for 32c ATAC-seq data, while read density enrichment decreased for 32C H3K27ac histone mark (Figure 2A, B).

Since there was a high degree of read density enrichment between OVO ChIP and other chromatin marks/low nucleosome density we wanted to determine the extent of the overlap between significant OVO ChIP peaks and significantly called peaks from the different types and stages of histone marks and ATAC-seq data. To do this, we measured the relative distance of OVO ChIP peaks to the same datasets described above. We found that OVO ChIP peaks had a lower relative distance, and thus were spatially overlapping/closer in the genome, to 32c NC ATAC, GSC ATAC, GSC H3K27ac, GSC H3K4me3, and 32c NC H3K27ac peaks, in that order (Figure 2C). While the relative distance between OVO ChIP peaks and H3K9me3 and H3K27me3, regardless of stage, showed no spatial association. There was also further support for this association with transcriptionally active histone marks/open chromatin when measuring the overlap between significant OVO ChIP peaks and the respective significant histone ChIP and ATAC-seq peaks (Figure 2D). A Fisher's exact test indicated a significant enrichment in overlapping peaks genome-wide between OVO and GSC ATAC ($p < 0.001$, odds ratio = 75.9), 32c NC ATAC ($p < 0.001$, odds ratio = Infinite), GSC H3K27ac ($p < 0.001$, odds ratio = 31.7), GSC H3K4me3 ($p < 0.001$, odds ratio =12.0), and 32c NC H3K27ac ($p < 0.001$, odds ratio = 7.9) peaks. While there was a significant depletion in overlapping peaks genome-wide between OVO and 32c NC H3K27me3 ($p < 0.001$, odds ratio = 0.6), GSC H3K9me3 ($p < 0.001$, odds ratio = 0.7), and 8c NC H3K9me3 ($p < 0.001$, odds ratio = 0.5).

The association of OVO binding with active histone marks and open chromatin was striking, but open chromatin is likely a general phenomenon of promoters (Haines and Eisen, 2008). Indeed, when measuring the read density for GSC and 32C ATAC-seq for OVO bound and OVO non-bound promoters, there is an enrichment for open chromatin at the TSS regardless of OVO binding. However, we did notice an increase in enrichment for OVO bound promoters compared to OVO non-bound promoters (Figure S1G), possibly suggesting that OVO bound promoters are more open or have an increase in accessibility when compared to non-OVO bound promoters. This same relationship held true for the transcriptionally active histone mark H3K27ac in GSCs (Figure S1H). Since only 45% of OVO ChIP peaks overlapped

336 TSSs, we plotted the read density of the above chromatin marks over OVO ChIP peak maximums for
337 OVO bound over the TSS, gene body, or intergenic regions (Figure S2A-D). We found that OVO bound
338 regions that were not overlapping the TSS still showed the same propensity for enrichment of open
339 chromatin and active histone marks. Intergenic regions were especially enriched for open chromatin
340 measured through ATAC-seq. Altogether suggesting that OVO binding genome-wide is tightly associated
341 with open chromatin regardless of germ cell stage, and active transcription in GSCs. In other words,
342 chromatin state data suggests OVO is acting positively on its target genes and raises the possibility that
343 OVO-binding and open chromatin are related.
344
345 <u>OVO DNA Binding Motifs are Evenly Distributed Around Promoters and are Enriched for INR, DPE, and</u>
346 <u>MTE Elements</u>
347 Our data thus far clearly indicates that OVO binding occurs at or very near the core promoter, a region
348 recognized by an enormous collection of factors that associate with RNA polymerase to initiate
349 transcription (Aoyagi and Wassarman 2000; Vo Ngoc, Kassavetis, and Kadonaga 2019). The highly
350 organized polymerase complex has sequence-specific DNA recognition sites with incredibly precise
351 spacing between them, with an overall DNA footprint of a little less than 100bp (Rice, Chamberlin, and
352 Kane 1993; FitzGerald et al. 2006; Ohler et al. 2002). There are upstream binding sites such as TATA,
353 sites at transcription start, such as the initiator (INR), and downstream promoter elements (DPE) (Vo
354 Ngoc, Kassavetis, and Kadonaga 2019). The combinations of these DNA motifs is not random in
355 mammals and Drosophila (FitzGerald et al. 2006), and distinct combinations of different motifs at the TSS
356 of genes expressed in *Drosophila* are conserved over tens of millions of years of evolution (Chen et al.
357 2014). The male germline expresses a number of TATA-associated factors that have been implicated in
358 male-specific promoter usage for gene expression (M. Hiller et al. 2004; M. A. Hiller et al. 2001; Lu et al.
359 2020; V. C. Li et al. 2009). It is possible that OVO is a female germline specific TATA-associated factor,
360 and if so, OVO binding sites at core promoters should share precise spacing with other core promoter
361 elements, suggesting it is likely part of the complex. If not, then OVO is more likely to facilitate binding of
362 the basal transcriptional machinery. Because of the extended footprint of engaged RNA polymerase,
363 OVO and the basal machinery would not be likely to occupy the same region at the same time.
364
365 Like OVO chip peaks, OVO DNA binding motifs were highly enriched at or near the TSS (Figure 3A). We
366 carefully analyzed the spacing of these sites relative to core promoter elements to see if spacing was
367 precise at the nucleotide level. We first searched for the presence of previously defined DNA motifs that
368 are enriched at promoters (FitzGerald et al. 2006; Ohler et al. 2002; Lim et al. 2004) using FIMO (Grant,
369 Bailey, and Noble 2011). We defined promoters by using the DNA sequences 150 nucleotides upstream
370 and downstream of the significant dominant TSSs in our previously analyzed ovary CAGE-seq datasets
371 (Chen et al. 2014). After extracting these sequences and searching for significant scoring motifs, we
372 plotted the density of each motif in relation to the empirically mapped TSSs (Figure 3B). We also
373 searched for all OVO motifs found in our significant ChIP peaks within these promoter sequences. When
374 plotting the density of DNA motifs found in ovary CAGE-seq promoters, we found that there were
375 prominent peaks for INR and M1BP (M1BP (J. Li and Gilmour 2013) = Ohler 1 (Ohler et al. 2002) = DMv4
376 (FitzGerald et al. 2006)) near the TSS, and MTE (Lim et al. 2004) and DPE elements downstream of the
377 TSS. This distribution and frequency are consistent with the constrained location of these DNA motifs
378 (FitzGerald et al. 2006; Ohler et al. 2002; Chen et al. 2014). Significantly, the OVO DNA binding motifs
379 showed a broad distribution upstream and downstream of the TSS.
380
381 The precise core promoter architecture of OVO bound TSSs is revealed in the CAGE-seq dataset.
382 Plotting the distribution of classical core promoter sequence elements in OVO bound promoters showed a
383 similar, but exaggerated, profile compared to all core promoters of the ovary CAGE-seq dataset. We
384 found a significant enrichment for INR ($p < 0.01$, odds ratio = 1.70), DPE ($p < 0.01$, odds ratio = 1.81),
385 MTE ($p < 0.01$, odds ratio = 1.65), and most importantly, OVO DNA binding motifs ($p < 0.01$, odds ratio =
386 4.83), in ovary promoters that overlapped an OVO ChIP peak in comparison to the subset of ovary
387 promoters that did not overlap an OVO ChIP peak (Figure 3C, 3D). This indicates that OVO bound
388 promoters are more likely to contain these specific promoter elements than non-OVO bound promoters.
389 As has been described before, promoters containing INR and DPE, but lacking TATA-box elements, are
390 common among *Drosophila* gonad promoters compared to promoters of other tissue types (Chen et al.
391 2014). The presence of TATA-box elements is negatively associated with germline-specific gene

392 expression (FitzGerald et al. 2006). We found that TATA-box elements were significantly depleted in
393 ovary CAGE-seq promoters when compared to testes ($p < 0.01$, odds ratio = 0.78) (Figure 3E) or
394 digestive system ($p < 0.01$, odds ratio = 0.50) (Figure 3F) CAGE-seq promoters. Indeed, both *ovo* and *otu*
395 have TATA-less promoters. Briefly, OVO bound promoters are characterized by the presence of INR,
396 DPE, MTE, and, of course, OVO DNA binding motifs. This could represent a functional class of promoters
397 utilized for gene expression in the *Drosophila* ovary. Importantly, the distribution of OVO DNA binding
398 motifs in ovary promoters is not fixed relative to TSSs or other core promoter elements. Thus, it is highly
399 unlikely that OVO acts as a female germline RNA Polymerase complex member that anchors the complex
400 to the core promoter and helps determine the +1 mRNA nucleotide. Rather, the imprecise location of
401 OVO binding sites might suggest that OVO is more likely to facilitate the binding of other basal
402 transcriptional factors.
403
404 <u>OVO Activates Gene Expression in the Female Germline</u>
405 Occupancy is a requirement for activity, but occupancy does not equal activity. Understanding the
406 transcriptional consequences of OVO occupancy genome-wide would allow us to investigate
407 mechanisms. However, as we mentioned earlier, the fact that *ovo* is absolutely required for female
408 germline viability greatly complicates this analysis. Measuring gene expression in dead or dying germ
409 cells was unlikely to be informative. Previous work from our lab has identified a transheterozygous *ovo*
410 allelic combination ($ovo^{ovo\text{-}GAL4}/ovo^{\Delta BP}$) that greatly reduces OVO activity resulting in sterility, however,
411 female germ cells are able to survive up until at least stage 5 of oogenesis (Benner et al. 2023). $ovo^{ovo\text{-}}$
412 ^{GAL4} is a CRISPR/Cas9 derived T2A-GAL4-3xSTOP insertion upstream of the splice junction of exon 3 in
413 the *ovo-RA* transcript (Figure S1A). Importantly, this insertion in the extended exon 3 would disrupt
414 roughly 90% of the *ovo-B* transcripts. However, since about 10% of *ovo-B* transcripts utilize an upstream
415 splice junction in exon 3, these transcripts would not be disrupted with the T2A-GAL4-3xSTOP insertion
416 and thus allow for enough OVO activity for germ cell survival (Benner et al. 2023). Since $ovo^{ovo\text{-}GAL4}$
417 expresses GAL4 in place of full length OVO due to the T2A sequences, we can drive expression of a
418 rescuing OVO-B construct downstream of *UASp* to generate OVO^{+} female germ cells, which in fact does
419 rescue the arrested germ cell phenotype of $ovo^{ovo\text{-}GAL4}/ovo^{\Delta BP}$ ovaries. Therefore, in order to determine
420 genes that are transcriptionally responsive to OVO, we compared the gene expression profiles in sets of
421 ovaries that had the *ovo* hypomorphic phenotype with a negative control rescue construct ($ovo^{ovo\text{-}}$
422 $^{GAL4}/ovo^{\Delta BP}$; *UASp-GFP*)(Figure 4A) versus those that drive expression of the rescue construct expressing
423 OVO-B ($ovo^{ovo\text{-}GAL4}/ovo^{\Delta BP}$; *UASp-3xFHA-OVO-B*)(Figure 4B).
424
425 Since $ovo^{ovo\text{-}GAL4}/ovo^{\Delta BP}$; *UASp-3xFHA-OVO-B* females have full rescue of the arrested germ cell
426 phenotype seen in $ovo^{ovo\text{-}GAL4}/ovo^{\Delta BP}$; *UASp-GFP* females, we needed to take further measures to ensure
427 our analysis of gene expression was stage comparable between the two sets of ovaries. The adult female
428 ovary contains somatic cells, germline stem cells, and germline derived nurse cells that would be profiled
429 in a bulk ovary tissue RNA-seq experiment. Although OVO is only required and expressed in germline
430 derived cell types, we chose to dissect one day old post-eclosion $ovo^{ovo\text{-}GAL4}/ovo^{\Delta BP}$; *UASp-3xFHA-OVO-B*
431 female ovaries to enrich for early stages of oogenesis and collected only ovarioles containing the
432 germarium through previtellogenic egg chambers. $ovo^{ovo\text{-}GAL4}/ovo^{\Delta BP}$; *UASp-GFP* ovaries were collected
433 at the same age post-eclosion and we specifically collected ovaries that contained a visible ovariole
434 structure (and therefore contained germ cells) to minimize comparing germ cells to somatic ovary
435 structures, but rather germ cells to germ cells. We then performed RNA-seq in quadruplicate and
436 measured the changes in gene expression between ectopic rescue OVO and hypomorphic OVO ovaries.
437 We used a significance level of p-adj < 0.05 and a log2 fold change cutoff of >|0.5| to call differential
438 expression between these two sets of ovaries. We utilized these log2 fold change cutoffs for two reasons.
439 Our control ovary genotype ($ovo^{ovo\text{-}GAL4}/ovo^{\Delta BP}$; *UASp-GFP*) has hypomorphic OVO activity, hence germ
440 cells can survive but are arrested. With the addition of ectopic rescue OVO in $ovo^{ovo\text{-}GAL4}/ovo^{\Delta BP}$; *UASp-*
441 *3xFHA-OVO-B* ovaries, we predicted that genes that were directly regulated by OVO would
442 transcriptionally respond, however, we were unsure as to what degree the response would be in
443 comparison to hypomorphic OVO. We reasoned that if the changes were not significant between
444 genotypes, then minor changes in gene expression would not matter. Our second reason for using these
445 cutoffs is we had an internal control between the two genotypes. We knew through immunostaining that
446 Vas protein was present in the germline of both genotypes (Figure 4A, 4B) and therefore was likely
447 expressed at similar levels in the germline of both genotypes. Both genotypes also expressed *GAL4*

under the control of *ovo* in the germline. We examined the expression levels of *vas* and *GAL4* and found that *vas* had a log2 fold change of 0.15 (p-adj = 0.03) and *GAL4* had a log2 fold change of 0.33 (p-adj = 0.18) (Figure 4C). These data suggest a slight underrepresentation of germline expression in *ovo* hypomorphic ovaries. Therefore, by using the greater than 0.5 and less than -0.5 log2 fold change cutoffs, and a less than 0.05 p-adj value cutoff, we would be conservative to not call genes differentially expressed due to differences in the relative abundance of germ cells and somatic cells.

We were able to reliably detect the expression of 10,804 genes in these early ovarioles (Table S4). The differential expression analysis indicated that 1,994 genes primarily expressed in the germline (see next paragraph) significantly increased in expression with ectopic rescue OVO (Figure 4C, cyan/purple dots) and 2,924 genes primarily expressed in the soma (see next paragraph) significantly decreased in expression with ectopic rescue OVO expression (Figure 4C, yellow/blue dots). 5,886 genes were not considered to be differentially expressed in our analysis (Figure 4C, gray dots). OVO is expressed in the germline, not the soma, and previous work has shown that OVO-B is a transcriptional activator (Andrews et al. 2000), so we hypothesized that many of the genes increasing in expression in the presence of rescuing OVO were direct downstream targets. We found that 2,298 genes that were expressed in our RNA-seq data overlapped an OVO ChIP peak. 666 genes significantly increased in expression and were bound by OVO, which is a significant enrichment according to a Fisher's exact test (Figure 4C, cyan dots, $p < 0.01$, odds ratio = 2.21). While conversely, 564 genes decreased in expression and were bound by OVO, indicating a significant depletion according to a Fisher's exact test (Figure 4C, blue dots, $p < 0.01$, odds ratio = 0.85). This strongly suggests that genes that are bound by OVO, transcriptionally respond in a positive manner. This finding is fully consistent with our meta-analysis comparing OVO ChIP-seq and histone ChIP/ATAC-seq data (Figure 4E). OVO binding was highly associated with transcriptionally active histone marks such as H3K27ac and H3K4me3, open chromatin, and increased expression.

There are genes that showed decreased expression in the OVO rescued ovaries, but we believe this is technical rather than biological. OVO is expressed only in the germline, but ovarioles contain germ cells and somatic cells. The presence of empty ovarioles, containing leftover strings of somatic cells, are evident even in $ovo^{ovo\text{-}GAL4}/ovo^{\Delta BP}$; *UASp-GFP* ovaries that contain germ cells. Conversely, $ovo^{ovo\text{-}GAL4}/ovo^{\Delta BP}$; *UASp-3xFHA-OVO-B* ovaries are fully rescued, and therefore possess more germ cell containing ovarioles than $ovo^{ovo\text{-}GAL4}/ovo^{\Delta BP}$; *UASp-GFP* ovaries (Benner et al. 2023). Despite our best efforts to dissect individual ovarioles with a full complement of germ cells and egg chambers, we wondered if there might be fewer germ cells and egg chambers in the $ovo^{ovo\text{-}GAL4}/ovo^{\Delta BP}$; *UASp-GFP* ovaries. To confirm that genes increasing in expression in ectopic rescue OVO were germline derived, we cross-referenced the significantly expressed genes in our RNA-seq datasets with the modENCODE developmental RNA-seq datasets (Graveley 2010). We extracted the gene names of all genes that were considered to be 'moderately expressed' in 0-2 hour old embryos, which are produced during oogenesis and are deposited into the early embryo. We found that 71% of genes (1,409/1,994) that had a significant increase in expression in the presence of ectopic rescue OVO were found to be expressed in 0-2 hour old embryos (Figure 4D, green dots), while only 21% of genes (625/2,924) that had a significant decrease in expression were found in the same embryo dataset (Figure 4D, yellow dots). 3,448 genes from the 0-2 hour old embryo dataset were not differentially expressed in our RNA-seq dataset (Figure 4D, purple dots). A Fisher's exact test confirmed that there was a significant enrichment for genes that significantly increased in expression and were present in 0-2 hour old embryos ($p < 0.01$, odds ratio = 2.8). In comparison, there was a significant depletion for genes that significantly decreased in expression and were present in 0-2 hour old embryos ($p < 0.01$, odds ratio = 0.17). This result indicated that genes that significantly increased in expression were more likely to be expressed in the germline and that the presence of ectopic rescue OVO significantly increased the expression of genes that were maternally deposited in the early embryo. While the set of genes that significantly decrease in expression are not enriched in the embryo and are more likely specific to somatic cell gene expression. These genes are unlikely to be direct OVO targets due to the absence of OVO in those cells, although we certainly cannot rule out the possibility of a non-autonomous effect of OVO on somatic gene expression. In terms of the germline proper, OVO appears to be a positively acting transcription factor.

<u>OVO Positively Regulates Essential Oogenesis Genes</u>

503 We wanted to examine a subset of the OVO target genes in detail, and began with the known OVO
504 targets, *ovo* itself and *otu* (Bielinska et al. 2005; Lü et al. 1998; Lü and Oliver 2001). Since the
505 relationship between OVO binding to these two genes has been well-characterized, we validated the
506 OVO ChIP, histone ChIP/ATAC-seq, and RNA-seq datasets by examining these two genes first. Since
507 OVO positively regulates the expression of both these genes, then we would expect OVO to be physically
508 bound at OVO motifs required for high transcription, the presence of transcriptionally active histone marks
509 and open chromatin at these loci, as well as a positive transcriptional response in the presence of
510 rescuing OVO-B. This is exactly what we observed. A significant OVO ChIP peak was found overlapping
511 the TSS of *ovo-B*, with four significant OVO DNA binding motifs present (Figure 5A). ATAC-seq,
512 H3K27ac, and H3K4me3 peaks overlapped the *ovo* promoter. Transcriptionally, *ovo* RNA-seq reads are
513 likely derived from the *UASp-3xFHA-OVO-B* cDNA rescue or are indistinguishable between the genomic
514 locus and rescuing cDNA transgene. We found a non-significant increase in exon 3 to exon 4 intronic *ovo*
515 reads with the expression of ectopic rescue OVO (log2 fold change = 0.76, p-adj = 0.26). These intronic
516 reads would be derived from the endogenous *ovo* locus, but it is difficult to conclusively determine if the
517 endogenous *ovo* locus would respond transcriptionally to ectopic OVO downstream of *UASp* (for
518 example, the pathway for *ovo* is no longer autoregulatory in $ovo^{ovo\text{-}GAL4}/ovo^{\Delta BP}$; *UASp-3xFHA-OVO-B*
519 germ cells, there is an additional GAL4>*UASp* activation step). So, we could not confidently assess
520 whether *ovo* responded transcriptionally to ectopic rescue OVO. However, when looking at the *otu* locus
521 (Figure S3), we found OVO occupancy over the TSS of both annotated *otu* promoters, with significant
522 OVO DNA binding motifs overlapping and in close proximity to the TSSs. The *otu* locus contained similar
523 ATAC-seq and activating histone mark peaks overlapping the TSS found at the *ovo* locus. It was also
524 evident that *otu* had a positive transcriptional response to the presence of OVO rescue (log2 fold change
525 = 2.41; p-adj < 0.001). These results confirm that OVO binds and positively regulates both itself and *otu in*
526 *vivo*, as previous work has indicated.
527
528 Since our overlapping OVO ChIP-seq and RNA-seq data suggests that hundreds of genes that are bound
529 by OVO increase in expression in the presence of ectopic rescue OVO, we wanted to know more about
530 the functions of those genes. To do this, we performed Gene Ontology enrichment analysis with gProfiler
531 software (Raudvere et al. 2019). To be especially stringent, we focused on the genes that contained an
532 OVO ChIP peak overlapping the transcriptional start site and significantly increased in expression in the
533 presence of rescue OVO. 525 genes met these criteria. Biological process GO term enrichment analysis
534 on these 525 genes showed a significant enrichment for 45 GO terms (Table S5). The significant GO
535 terms were almost exclusively related to female reproduction and maternal control of early embryonic
536 development (Figure 6A). Genes that are required for processes such embryonic axis specification,
537 mRNA localization, egg activation, and translational regulation were found within these significantly
538 enriched GO terms. These GO terms are well understood in the context of oogenesis and broadly
539 suggest that OVO expression in adult gonads is essential for constructing an egg and depositing maternal
540 RNAs to support zygotic embryonic development.
541
542 GO term enrichment analysis of genes that are bound by OVO and increase in expression in the
543 presence of ectopic rescue OVO suggested that OVO is likely a main transcriptional regulator of
544 oogenesis. These genes are the subject of decades of work on *Drosophila* oogenesis, but essentially all
545 the work on them has focused on what they do, not on how they are transcriptionally regulated. For
546 example, *bicoid* (Figure 6B), and *bicoid* mRNA binding proteins *exuperantia* (*exu*) and *swallow* (*swa*), are
547 essential for anterior specification of the embryo (Lasko 2012). All these genes were occupied by OVO *in*
548 *vivo*, significantly upregulated by OVO-B, and had OVO motifs in close proximity to the TSS. Genes
549 involved in posterior patterning (*oskar* and *nanos*) (Figure 6C), as well as pole cell specification genes
550 (*polar granule component*, *germ cell-less*, and *aubergine*)(Lasko 2012; L. Benner, Deshpande, and Lerit
551 2018), also showed similar RNA-seq, ChIP-seq, and OVO DNA binding motif profiles as *ovo* and *otu*.
552 Genes that are involved in translational silencing and regulation of maternally provided mRNAs, such as
553 *cup* (Figure 6D), *maternal expression at 31B* (*me31B*), *oo18 RNA-binding protein* (*orb*), and *bruno 1*
554 (*bru1*), as well as essential genes involved in meiosis completion and egg activation after fertilization
555 (*giant nuclei* (*gnu*), *pan gu* (*png*), *plutonium* (*plu*), *wispy* (*wisp*), *C(3)G*, and *matrimony* (*mtrm*)) (Figure
556 6E)(Lasko 2012; Avilés-Pagán and Orr-Weaver 2018) all show this stereotypic pattern of promoter
557 proximal OVO occupancy and DNA binding motifs, and OVO-dependent transcription. These data

558 indicate that the OVO is a central transcription factor activating the expression of essential maternal and
559 early embryonic development pathways in the female germline.
560
561 We also found that the genes *fs(1)N*, *fs(1)M3*, and *closca*, were all bound by OVO and responded
562 transcriptionally to the presence of ectopic rescue OVO. These genes are significant because they
563 constitute a set of genes that are expressed in the germline and the encoded proteins are eventually
564 incorporated into the vitelline membrane providing the structural integrity and impermeability of the egg
565 (Mineo, Furriols, and Casanova 2017; Ventura et al. 2010). Loss-of-function of these three genes results
566 in flaccid eggs that are permeable to dye and fail to develop. The loss-of-function phenotype of *fs(1)N*,
567 *fs(1)M3*, and *closca* closely resembles the dominant antimorph ovo^{D3} phenotype. The ovo^{D3} allele is the
568 weakest of the original dominant-negative *ovo* alleles and produces defective eggs allowing us to explore
569 the role of OVO in late stages (Busson et al. 1983; Komitopoulou et al. 1983). ovo^{D3}/ovo^{+}
570 transheterozygous females express a repressive form of OVO that results in dominant sterility, and
571 importantly, these females lay flaccid eggs with compromised vitelline membranes that are permeable to
572 the dye neutral red (Oliver, Pauli, and Mahowald 1990). Since OVO^{+} is bound at the TSS of *fs(1)N*,
573 *fs(1)M3*, and *closca*, and these three genes respond transcriptionally to OVO^{+}, then it is plausible that the
574 repressive OVO^{D3} is negatively regulating these three genes that are required for vitelline membrane
575 formation. This is evidence that OVO is not only involved in regulating the expression of numerous
576 essential maternal pathways for embryonic development, but it is also essential for regulating genes that
577 are required for egg integrity and maturation.
578
579 **Discussion**
580 Since its original isolation as a dominant female sterile locus in Drosophila (Busson et al. 1983;
581 Komitopoulou et al. 1983), o*vo* has long been known as an essential gene in oogenesis. Female germ
582 cells require *ovo* for survival and differentiation, while it has no described roles or functions in the male
583 germline (Oliver, Perrimon, and Mahowald 1987; Oliver, Pauli, and Mahowald 1990). OVO has also been
584 found to be eternally present in the female germline, attesting to its likely continual requirement for female
585 germ cell viability and identity (Benner et al. 2023). Our work here significantly expands our knowledge on
586 OVO function in the female germline, showing that OVO binds and positively regulates a large array of
587 genes required to build an egg and pattern the resulting embryo after fertilization. OVO accomplishes this
588 by directly binding to the promoters of its targets, as well as more distant sites that could represent
589 enhancers. Altogether, we suggest that OVO is a master transcriptional regulator coordinating a number
590 of essential maternal pathways involved in oocyte and early embryonic development. Hints of these
591 functions can be found in the hypomorphic and antimorphic *ovo* alleles which show egg chamber arrest,
592 ventralized eggs, and permeable vitelline membranes. It is clear that OVO is required to activate multiple
593 pathways involved in oocyte and early embryonic development.
594
595 The GO term enrichment analysis on genes that were bound by OVO and transcriptionally responded to
596 OVO surprisingly indicated a large degree of overlap in oocyte and early embryonic developmental
597 pathways. Also, OVO seemed to reinforce these pathways at multiple key genes within each pathway.
598 For example, OVO bound to the promoters and increased the expression of *bcd*, and the *bcd* mRNA
599 binding proteins *exu* and *swa*, all involved in ensuring correct anterior specification of the embryo (Lasko
600 2012). Genes that are essential for egg activation were coordinately regulated by OVO as well. OVO
601 downstream target genes *gnu*, *png*, *plu*, and *wisp* all belong in the same interconnected pathway
602 ensuring egg activation (Avilés-Pagán and Orr-Weaver 2018). A similar story was found for genes such
603 as *cup*, *Me31b*, *bru1*, and *orb*, indicating that OVO controls a battery of genes involved in the positive
604 regulation of RNA binding proteins that negatively regulate translation (Lasko 2012). OVO also bound and
605 positively regulated a number of posterior and germ plasm specification genes such as *osk*, *nos*, *aub*, *gcl*,
606 and *pgc* (Lasko 2012; Mahowald 2001). Given this plethora of famous maternal effect loci, it might be
607 tempting to suggest that OVO is sufficient for egg production, but there are important exceptions. For
608 example, other important germ plasm factors such as *staufen* and *tudor* were not bound by or
609 transcriptionally responsive to OVO. This observation suggest that other transcription factors are
610 responsible for regulating these genes.
611
612 OVO binds in close proximity to the TSS of genes it positively regulates, however, it is still unclear
613 precisely how it regulates gene expression. The possibilities include integration into the RNA Polymerase

complex itself, a short distance sigma factor like function, a core promoter conditioning function (pioneering), and/or garden variety transcription factor. Although active core promoters specifically in the ovary are enriched for OVO DNA binding motifs, we did not find a strict spatial orientation for these motifs in relation to the TSS, such as is found with other DNA elements such as INR, DPE, and MTE (Ohler et al. 2002; FitzGerald et al. 2006; Lim et al. 2004). It is therefore unlikely that OVO is a core component of the RNA Polymerase complex in the female germline. This suggests that it is unlikely to be analogous to male specific TATA-associated factors that have been shown to activate gene expression in the male germline (M. Hiller et al. 2004; M. A. Hiller et al. 2001; Lu et al. 2020; V. C. Li et al. 2009). It is therefore possible, and previously well supported, that OVO is an activator of transcription (Lü et al. 1998; Lü and Oliver 2001; Bielinska et al. 2005). One aspect of OVO DNA binding that showed differences with stage-specific histone ChIP and ATAC-seq, was OVO's strong association with open chromatin. The role of repressors of transcription such as the polycomb complex, *egg*, *wde*, and *Su(var)205* in restricting gene expression through promoting heterochromatin formation in differentiating egg chambers is well established (Smolko, Shapiro-Kulnane, and Salz 2018; DeLuca et al. 2020). OVO might ensure that the chromatin status of maternally expressed genes remains open. Evidence from our work points to OVO fulfilling that role.

In GSCs OVO ChIP peaks largely overlap open chromatin and transcriptionally active histone marks. However, in stage 5 egg chambers, there was an even higher degree of association with open chromatin (almost all OVO ChIP peaks overlapped ATAC-seq peaks), while the significant association with H3K27ac marks was greatly reduced. This difference is likely significant. As GSCs differentiate they accumulate repressive chromatin marks while the number of ATAC-seq and H3K27ac peaks are reduced. This increase in association with open chromatin and OVO binding, even as the amount of open chromatin is reduced throughout egg chamber differentiation, might indicate that OVO binding helps to maintain chromatin accessibility, even when the locus in question is no longer actively transcribed. The loss of histone marks of active transcription at OVO-bound open chromatin in later differentiating egg chambers might mean that OVO does not influence the transcriptional potential of target genes as strongly as it influences the chromatin status in this second phase. Therefore, OVO might be more similar in function to pioneer factors/chromatin remodelers than it is to a transcription factor that is only involved in activating transcription.

The requirement for OVO at the TSS of target genes has been well characterized at its own locus as well as its downstream target *otu*. Our OVO ChIP and expression data confirm findings from previous work that OVO is binding to these target promoters, and in the case of *otu*, strongly responds transcriptionally to the presence of OVO. Although we did not test the requirement for OVO DNA binding motifs at other OVO bound genes in this work, this has been extensively explored before, showing that removal of OVO DNA binding sites overlapping the TSS results in a strong decrease in reporter expression (Lü et al. 1998; Bielinska et al. 2005; Lü and Oliver 2001). Removal of more distal upstream OVO DNA binding sites also reduces reporter expression to a lesser degree. However, for most cases tested, removal of OVO DNA binding sites while leaving the rest of the enhancer regions intact, never totally abolished reporter expression. These dynamics are highly similar to work that has been completed on the pioneer factor *zelda* (*zld*). Adding *zld* DNA binding motifs to a stochastically expressed transcriptional reporter increases the activity and response of the reporter (Dufourt et al. 2018). Distally located *zld* DNA binding motifs influenced reporter expression to a lesser degree than proximal sites. A single *zld* DNA binding site adjacent to the TSS produced the strongest reporter activity. Importantly, just like the activity of OVO transgenic reporters, there is not an absolute requirement for *zld* DNA binding to activate reporter expression, however, the addition of TSS adjacent *zld* DNA binding motifs does strongly influence reporter response. We know that *zld* achieves this reporter response through its pioneering activity (Xu et al. 2014; Harrison et al. 2011), whether OVO achieves this similar effect on gene expression through a shared mechanism, or in cooperation with other transcription factors needs to be further explored.

Methods

All reagents used in this study can be found in the FlyBase recommended supplementary ART table (Table S6).

Fly Husbandry

670 All fly crosses were conducted at 25°C with 65% relative humidity and constant light unless otherwise
671 noted. Flyfood consisted of premade flyfood (D20302Y) from Archon Scientific (Durham, NC).
672
673 Immunofluorescence and Image Analysis
674 All immunostaining procedures were done as previously described (Benner et al. 2023). Antibodies and
675 their respective dilutions are indicated in Table S6. Imaging was also completed as previously described
676 (Benner et al. 2023).
677
678 RNA-seq library preparation and sequencing
679 Twenty, one day old post-eclosion *ovo*$^{\Delta BP}$/*ovo*$^{ovo\text{-}GAL4}$; *UASp-GFP* and *ovo*$^{\Delta BP}$/*ovo*$^{ovo\text{-}GAL4}$; *UASp-3xFHA-*
680 *OVO-B* ovaries were dissected and germariums through previtellogenic egg chambers were removed with
681 microdissection scissors and placed in ice cold PBS making up one biological replicate. RNA was then
682 extracted from four biological replicates with a Qiagen RNeasy Plus Kit (Qiagen) according to the
683 manufacturer's protocol, eluted in dH_2O, and RNA concentrations were measured with Quant-iT
684 RiboGreen RNA Assay Kit (ThermoFisher Scientific). 500 ng of total RNA was then used to make RNA-
685 seq libraries with an Illumina Stranded mRNA Prep Kit according to the manufacturer's protocol (Illumina).
686 IDT for Illumina RNA UD Indexes Set A were used. Library concentrations were measured with Quant-iT
687 PicoGreen dsDNA Assay Kit (ThermoFisher Scientific), pooled, and then 50 nucleotide paired-end DNA
688 sequencing was completed on an Illumina NovaSeq 6000 system using a S1 flow cell (Illumina). Raw
689 RNA-seq reads are available at the SRA (SAMN38284748-SAMN38284755).
690
691 ChIP-seq library preparation and sequencing
692 Adult *ovo*$^{Cterm\text{-}3xFHA}$ and *ovo*$^{Cterm\text{-}GFP}$ females were collected and fed for 24 hours before ovaries were
693 dissected. 50 dissected ovaries were placed in ice cold phosphate buffered saline (PBS, Gibco,
694 ThermoFisher Scientific) and then incubated in 1 mL crosslinking solution containing 2% formaldehyde
695 (Pierce, ThermoFisher Scientific) (50mM HEPES Buffer, 1mM EDTA, 0.5 mM EGTA, 100mM NaCl), and
696 rotated at 37°C for 20 minutes. Ovaries were then incubated in 1 mL stop solution (125mM Glycine,
697 0.01% Triton X-100 (Millipore Sigma), diluted in PBS) and rotated for 5 minutes at room temperature.
698 Ovaries were then washed twice with 1 mL ice cold wash buffer (0.01% Triton X-100 in PBS) for 5
699 minutes. The last wash was removed, and ovaries were stored at -80°C until future processing. Once all
700 samples were collected, 4x50 ovaries were then homogenized in 250 µL RIPA lysis buffer (Pierce,
701 ThermoFisher Scientific) containing 1x protease inhibitor cocktail (cOmplete Mini Protease Inhibitor
702 Cocktail, Roche, Millipore Sigma) and 1 mM PMSF (Roche, Millipore Sigma) and kept on ice for 10
703 minutes. 40mg of 212-300 µm acid-washed glass beads (Millipore Sigma) were then added to
704 homogenized ovary lysate. Samples were then sonicated with a Bioruptor Pico sonication device
705 (Diagenode) at 4C for 15 cycles of 30 seconds on and 30 seconds off. Sonicated lysate was then
706 transferred to a new tube and centrifuged at 13,300 rpm for 10 minutes at 4°C. Three supernatants were
707 then combined to form one biological replicate. 100 µL for each biological replicate was removed and
708 stored at -80°C for input control. To pull down C-terminally tagged OVO, 100 µL of monoclonal anti-HA-
709 agarose (Millipore Sigma) or 50 µL of ChromoTek GFP-Trap agarose (Proteintech) were washed three
710 times with RIPA lysis buffer and spun down at 1,200 RPMs for one minute at 4°C. 550 µL of *ovo*$^{Cterm\text{-}3xFHA}$
711 supernatant was added to monoclonal anti-HA-agarose and 550 µL of *ovo*$^{Cterm\text{-}GFP}$ supernatant was added
712 to ChromoTek GFP-Trap agarose. Samples were supplemented with 1x protease inhibitor cocktail and 1
713 mM PMSF and incubated on a rotator at 4°C overnight.
714
715 The next day, agarose was washed in a stepwise fashion with solutions from a Chromatin
716 Immunoprecipitation Assay Kit (Millipore Sigma), beginning with 1 mL of a low salt wash buffer, high salt
717 wash buffer, LiCl buffer, and ending with 2 washes in 0.1x TE buffer. 300 µL of freshly prepared ChIP
718 elution/decrosslinking solution (1% SDS, 100mM $NaHCO_3$, 250 mM NaCl, 10mM EDTA, 50 mM Tris-HCl,
719 200 µg/mL Proteinase K) was added to the pelleted agarose, or 200 µL of chip elution/decrosslinking
720 solution was added to 100 µL input control and incubated at 65°C overnight. DNA was extracted by
721 adding 300 µL phenol:chloroform:iso-amyl alcohol (125:24:1) (Millipore Sigma). The samples were
722 vortexed for 30 seconds then centrifuged at 13,300 RPMs for 5 minutes at 4°C. The aqueous layer was
723 extracted, and this process was repeated once more. 1 µL glycogen (20 mg/mL), 30 µL 1M sodium
724 acetate, and 750 µL 100% EtOH was added to the extracted aqueous layer, vortexed, and incubated at -
725 20°C for 30 minutes. Solution was spun at 13,300 RPMs for 20 min at 4°C. Supernatant was removed

726 and the pellet was washed with 500 µL 70% EtOH and spun down at 13,300 RPMs for 20 minutes at 4°C.
727 This step was repeated but with 100% EtOH. The resulting pellet was briefly speedvacced and
728 resuspended in 50 µL dH_2O.
729
730 To make ChIP-seq libraries, DNA concentration for immunoprecipitated and input control samples were
731 measured with a Quant-iT PicoGreen dsDNA Assay Kit (ThermoFisher Scientific). 5 ng of DNA for each
732 sample was then used with the NEBNext Ultra II DNA Library Prep Kit for Illumina (New England Biolabs)
733 and completed according to the manufacturer's protocol. ChIP-seq library concentrations were then
734 measured with a Quant-iT PicoGreen dsDNA Assay Kit, pooled, and then 50 nucleotide paired-end DNA
735 sequencing was performed on an Illumina NovaSeq 6000 system using the XP workflow (Illumina). Raw
736 ChIP-seq reads are available at the SRA (SAMN38284736-SAMN38284747).
737
738 RNA-seq, ChIP-seq, CAGE-seq and Gene Ontology Analysis
739 For RNA-seq analysis of *ovo*$^{\Delta BP}$/*ovo*$^{ovo\text{-}GAL4}$; *UASp-GFP* and *ovo*$^{\Delta BP}$/*ovo*$^{ovo\text{-}GAL4}$; *UASp-3xFHA-OVO-B*
740 ovaries, 50 nucleotide paired-end reads were mapped to the FlyBase r6.46 genome (Gramates et al.
741 2022) for differential expression analysis and the BDGP Release 6 Drosophila Genome (dos Santos et al.
742 2015) for read level genome browser tracks using Hisat2 (-k 1 --rna-strandness RF --dta)(Kim et al.
743 2019). DNA sequences for *GAL4* and *GFP* were added to the FlyBase r6.46 genome as separate
744 chromosomes. Mapped reads were then sorted and indexed with Samtools (samtools sort and samtools
745 index)(Danecek et al. 2021). Gene level readcounts were then derived with htseq-count (-s reverse -r
746 pos)(Anders, Pyl, and Huber 2015) and used for differential expression analysis with DeSeq2 (Love,
747 Huber, and Anders 2014). Genes with 0 mapped reads were removed from the DESeq2 analysis.
748
749 For ChIP-seq analysis of OVO-HA, OVO-GFP, OVO-HA input, and OVO-GFP input samples, 50
750 nucleotide paired-end reads were mapped to the FlyBase r6.46 genome for peak calling analysis and the
751 BDGP Release 6 Drosophila Genome for read level genome browser tracks using Hisat2 (-k 1 --no-
752 spliced-alignment -X 900). Mapped reads were sorted using Samtools (samtools sort and samtools index)
753 and duplicate reads were removed with Picard (REMOVE_DUPLICATES=true)(broadinstitute, n.d.).
754 Significant ChIP peaks were called for OVO-HA and OVO-GFP versus their respective input controls
755 separately using Macs3 callpeak software (-g 1.2e8 -q 0.0001)(Zhang et al. 2008). Overlapping ChIP
756 peaks for OVO-HA and OVO-GFP were then determined with bedtools intersect software (Quinlan and
757 Hall 2010). Peak calling for GSC ATAC-seq (SRR24203655), 32c ATAC-seq (SRR24203650), GSC
758 H3K27ac (SRR11084657), H3K4me3 (SRR11084658), H3K27me3 (SRR11084656), H3K9me3
759 (SRR24203631), 8c NC H3K4me3 (SRR24203629), 32c NC H3K27ac (SRR24203635), and H3K27me3
760 (SRR11084652) ChIP-seq versus their respective input controls (SRR11084655, SRR11084651,
761 SRR24203634, SRR24203637) was conducted in the same manner as OVO ChIP-seq.
762
763 In order to generate gene-level read coverage tracks, deepTools' bamCompare software was used to
764 generate a single bigWig file comparing all replicates versus input controls (-bs 5 --effectiveGenomeSize
765 142573017 --normalizeUsing BPM --exactScaling --scaleFactorsMethod None)(Ramírez et al. 2016). The
766 bigWig file was then uploaded to UCSC genome browser for visualization (Kent et al. 2002).
767
768 To generate read coverage plots centered on the motif location or OVO peak maximums, genomic
769 locations of significant scoring motifs or peak maximums within overlapping OVO ChIP peaks were
770 determined and used as input for deepTools' computeMatrix reference-point (-a 2000 -b 2000 -bs 25 --
771 missingDataAsZero). Read density profiles for each motif or OVO peak maximum were then visualized
772 with deeptools plotProfile. In order to generate read coverage plots centered on the TSS, the same
773 methods as above were conducted except genes overlapping OVO ChIP peaks containing the respective
774 significant OVO DNA binding motifs were used as input instead.
775
776 In order to generate gene level read coverage heatmaps, deepTools' computeMatrix scale-regions
777 software was used to generate a single matrix for genes that were bound by OVO (-bs 25 --
778 missingDataAsZero -m 4000 --metagene). This matrix was then used as input for deepTools'
779 plotHeatmap software to generate heatmaps of ChIP-seq and RNA-seq for the given OVO binding
780 profiles centered on the TSS (--sortUsing max).
781

For CAGE-seq analysis, CAGE-seq libraries for ovary (SRR488283, SRR488282), testes (SRR488284, SRR488308, SRR488285, SRR488309), and male and female digestive system (SRR488289, SRR488288) tissues were downloaded and combined for each tissue type from the SRA. Reads were mapped to the BDGP Release 6 Drosophila Genome with Hisat2 (-k 1). Mapped reads were sorted with Samtools. Significant dominant TSSs were then determined with CAGEr software(Haberle et al. 2015) from sorted BAM files with getCTSS and annotated with annotateCTSS using the dm6.ensGene.gtf file(Hubbard et al. 2002) downloaded from UCSC(Kent et al. 2002). CAGE-seq reads were normalized with normalizeTagCount (ce, method = "simpleTpm", fitInRange = c(5, 40000), alpha = 1.15, T = 1*10^6) and then TSS clusters were determined with clusterCTSS (ce, threshold = 1, thresholdIsTpm = TRUE, nrPassThreshold = 1, method = "paraclu", maxDist = 20, removeSingletons = TRUE, keepSingletonsAbove = 5) in order to determine the dominant significant TSS for each respective tissue.

Gene ontology enrichment analysis was completed with g:Profiler's g:GOSt software (Raudvere et al. 2019) on the set of genes overlapping OVO ChIP peaks over the TSS and significantly upregulated in the presence of ectopic OVO (525 genes in total). All genes that were considered to be expressed in our RNA-seq datasets were used as a background control (10,801 genes in total). Default parameters were used for the enrichment analysis except for 'statistical domain scope' was set to 'custom' (our control background genes were uploaded here), 'significance threshold' was set to 'Bonferroni correction', and only GO biological process terms were searched for enrichment with the gene list. The GO terms listed in Figure 6 represent the 24 smallest GO term sizes according to Table S5.

Fisher's exact test was conducted for each respective analysis with the fisher.test() command in R (R Core Team 2021).

de novo Motif Enrichment and Promoter Motif Analysis

DNA sequences from significant overlapping OVO ChIP peaks were extracted from the Drosophila r6.46 genome and submitted to STREME software (Bailey 2021) of the MEME suite (Bailey et al. 2015). The default parameters were used for *de novo* motif enrichment analysis, including the use of shuffled input sequences as a control. After identifying 'OVO Motif One', OVO ChIP peaks that contained that sequence were removed and the resulting ChIP peaks were resubmitted for STREME analysis deriving derivative OVO DNA binding motifs like above. Significant OVO DNA binding motifs and *in vitro* OVO DNA binding motifs were searched in the BDGP Release 6 Drosophila Genome using FIMO (Grant, Bailey, and Noble 2011). In order to find significant DNA binding motif matches for 'OVO Motif One', this motif from STREME was submitted to Tomtom software (Gupta et al. 2007) of the MEME suite and searched within the JASPAR Core Insect database (2022)(Castro-Mondragon et al. 2022). XSTREME software was used with the default parameters to identify previously characterized and published DNA binding motifs within OVO ChIP peaks (Grant and Bailey 2021).

Promoter motif analysis was conducted by extracting the DNA sequences 200 nucleotides upstream and downstream of the significant dominant TSSs from CAGE-seq analysis for each respective tissue type. All common core promoter motifs (FitzGerald et al. 2006; Ohler et al. 2002) were then searched in these sequences depending on their strand specificity with the use of FIMO from the MEME suite using a p-value of < 0.003 for all non-OVO promoter motifs. All OVO motifs found in this study and through *in vitro* methods were also searched with the same method, except a p-value of < 0.0002 was used.

Data Availability

Drosophila strains used for this study are available upon request. All sequence information and datasets used in this study are in Table S6.

Acknowledgements

We would like to thank previous and current members of the Oliver lab, Laboratory of Biochemistry and Genetics at NIH, and L.B. committee members Mark Van Doren and Allan Spradling for insightful discussion and comments on this work throughout. Monoclonal antibodies were obtained from the Developmental Studies Hybridoma Bank, created by the Eunice Kennedy Shriver National Institute of Child Health and Human Development (NICHD) of the NIH and maintained at the Department of Biology, University of Iowa, Iowa City, IA 52242. Genetic and genomic information was obtained from FlyBase

(U41 HG-000739). This work utilized the computational resources of the NIH High-Performance Computing Biowulf cluster (http://hpc.nih.gov). Sequencing was completed by The National Heart, Lung, and Blood Institute (NHLBI) DNA Sequencing and Genomics Core.

Funding

This research was supported in part by the Intramural Research Program of the NIH, The National Institute of Diabetes and Digestive and Kidney Diseases (NIDDK) (awarded to B.O.). L.B. was supported by the NIH Graduate Partnership Program.

References

Anders, Simon, Paul Theodor Pyl, and Wolfgang Huber. 2015. "HTSeq--a Python Framework to Work with High-Throughput Sequencing Data." *Bioinformatics* 31 (2): 166–69.

Andrews, J., D. Garcia-Estefania, I. Delon, J. Lü, M. Mével-Ninio, A. Spierer, F. Payre, D. Pauli, and B. Oliver. 2000. "OVO Transcription Factors Function Antagonistically in the Drosophila Female Germline." *Development* 127 (4): 881–92.

Aoyagi, N., and D. A. Wassarman. 2000. "Genes Encoding Drosophila Melanogaster RNA Polymerase II General Transcription Factors: Diversity in TFIIA and TFIID Components Contributes to Gene-Specific Transcriptional Regulation." *The Journal of Cell Biology* 150 (2): F45–50.

Avilés-Pagán, Emir E., and Terry L. Orr-Weaver. 2018. "Activating Embryonic Development in Drosophila." *Seminars in Cell & Developmental Biology* 84 (December): 100–110.

Bailey, Timothy L. 2021. "STREME: Accurate and Versatile Sequence Motif Discovery." *Bioinformatics* 37 (18): 2834–40.

Bailey, Timothy L., James Johnson, Charles E. Grant, and William S. Noble. 2015. "The MEME Suite." *Nucleic Acids Research* 43 (W1): W39–49.

Bastock, Rebecca, and Daniel St Johnston. 2008. "Drosophila Oogenesis." *Current Biology: CB* 18 (23): R1082–87.

Benner, L., G. Deshpande, and D. A. Lerit. 2018. "Primordial Germ Cells of Drosophila Melanogaster." https://scholar.google.ca/scholar?cluster=7409236235465525669&hl=en&as_sdt=0,5&sciodt=0,5.

Benner, Leif, Elias A. Castro, Cale Whitworth, Koen J. T. Venken, Haiwang Yang, Junnan Fang, Brian Oliver, Kevin R. Cook, and Dorothy A. Lerit. 2019. "Drosophila Heterochromatin Stabilization Requires the Zinc-Finger Protein Small Ovary." *Genetics* 213 (3): 877–95.

Benner, Leif, Savannah Muron, and Brian Oliver. 2023. "Female Germline Expression of OVO Transcription Factor Bridges Drosophila Generations." *bioRxiv*. https://doi.org/10.1101/2023.08.25.554887.

Bielinska, Beata, Jining Lü, David Sturgill, and Brian Oliver. 2005. "Core Promoter Sequences Contribute to Ovo-B Regulation in the Drosophila Melanogaster Germline." *Genetics* 169 (1): 161–72.

Bishop, D. L., and R. C. King. 1984. "An Ultrastructural Study of Ovarian Development in the otu7 Mutant of Drosophila Melanogaster." *Journal of Cell Science* 67 (April): 87–119.

broadinstitute. n.d. "Picard." Picard. http://broadinstitute.github.io/picard/.

Busson, D., M. Gans, K. Komitopoulou, and M. Masson. 1983. "Genetic Analysis of Three Dominant Female-Sterile Mutations Located on the X Chromosome of DROSOPHILA MELANOGASTER." *Genetics* 105 (2): 309–25.

Castro-Mondragon, Jaime A., Rafael Riudavets-Puig, Ieva Rauluseviciute, Roza Berhanu Lemma, Laura Turchi, Romain Blanc-Mathieu, Jeremy Lucas, et al. 2022. "JASPAR 2022: The 9th Release of the Open-Access Database of Transcription Factor Binding Profiles." *Nucleic Acids Research* 50 (D1): D165–73.

Chen, Yu-Chien, Suewei I. Lin, Ying-Kuan Chen, Chuen-Sheue Chiang, and Gwo-Jen Liaw. 2009. "The Torso Signaling Pathway Modulates a Dual Transcriptional Switch to Regulate Tailless Expression." *Nucleic Acids Research* 37 (4): 1061–72.

Chen, Zhen-Xia, David Sturgill, Jiaxin Qu, Huaiyang Jiang, Soo Park, Nathan Boley, Ana Maria Suzuki, et al. 2014. "Comparative Validation of the D. Melanogaster modENCODE Transcriptome Annotation." *Genome Research* 24 (7): 1209–23.

Danecek, Petr, James K. Bonfield, Jennifer Liddle, John Marshall, Valeriu Ohan, Martin O. Pollard, Andrew Whitwham, et al. 2021. "Twelve Years of SAMtools and BCFtools." *GigaScience* 10 (2). https://doi.org/10.1093/gigascience/giab008.

DeLuca, Steven Z., Megha Ghildiyal, Liang-Yu Pang, and Allan C. Spradling. 2020. “Differentiating Drosophila Female Germ Cells Initiate Polycomb Silencing by Regulating PRC2-Interacting Proteins.” *eLife* 9 (August). https://doi.org/10.7554/eLife.56922.

Dufourt, Jeremy, Antonio Trullo, Jennifer Hunter, Carola Fernandez, Jorge Lazaro, Matthieu Dejean, Lucas Morales, et al. 2018. “Temporal Control of Gene Expression by the Pioneer Factor Zelda through Transient Interactions in Hubs.” *Nature Communications* 9 (1): 1–13.

FitzGerald, Peter C., David Sturgill, Andrey Shyakhtenko, Brian Oliver, and Charles Vinson. 2006. “Comparative Genomics of Drosophila and Human Core Promoters.” *Genome Biology* 7 (7): R53.

Gramates, L. Sian, Julie Agapite, Helen Attrill, Brian R. Calvi, Madeline A. Crosby, Gilberto Dos Santos, Joshua L. Goodman, et al. 2022. “FlyBase: A Guided Tour of Highlighted Features.” *Genetics* 220 (4). https://doi.org/10.1093/genetics/iyac035.

Grant, Charles E., and Timothy L. Bailey. 2021. “XSTREME: Comprehensive Motif Analysis of Biological Sequence Datasets.” *bioRxiv*. https://doi.org/10.1101/2021.09.02.458722.

Grant, Charles E., Timothy L. Bailey, and William Stafford Noble. 2011. “FIMO: Scanning for Occurrences of a given Motif.” *Bioinformatics* 27 (7): 1017–18.

Graveley, Brenton. 2010. “The Developmental Transcriptome of Drosophila Melanogaster.” *Genome Biology* 11 (Suppl 1): I11.

Gupta, Shobhit, John A. Stamatoyannopoulos, Timothy L. Bailey, and William Stafford Noble. 2007. “Quantifying Similarity between Motifs.” *Genome Biology* 8 (2): R24.

Haberle, Vanja, Alistair R. R. Forrest, Yoshihide Hayashizaki, Piero Carninci, and Boris Lenhard. 2015. “CAGEr: Precise TSS Data Retrieval and High-Resolution Promoterome Mining for Integrative Analyses.” *Nucleic Acids Research* 43 (8): e51.

Haines, Jenna E., and Michael B. Eisen. 2018. “Patterns of Chromatin Accessibility along the Anterior-Posterior Axis in the Early Drosophila Embryo.” *PLoS Genetics* 14 (5): e1007367.

Harms, E., T. Chu, G. Henrion, and S. Strickland. 2000. “The Only Function of Grauzone Required for Drosophila Oocyte Meiosis Is Transcriptional Activation of the Cortex Gene.” *Genetics* 155 (4): 1831–39.

Harrison, Melissa M., Xiao-Yong Li, Tommy Kaplan, Michael R. Botchan, and Michael B. Eisen. 2011. “Zelda Binding in the Early Drosophila Melanogaster Embryo Marks Regions Subsequently Activated at the Maternal-to-Zygotic Transition.” *PLoS Genetics* 7 (10): e1002266.

Hayashi, Makoto, Yuko Shinozuka, Shuji Shigenobu, Masanao Sato, Michihiko Sugimoto, Seiji Ito, Kuniya Abe, and Satoru Kobayashi. 2017. “Conserved Role of Ovo in Germline Development in Mouse and Drosophila.” *Scientific Reports* 7 (1): 1–10.

Hiller, M. A., T. Y. Lin, C. Wood, and M. T. Fuller. 2001. “Developmental Regulation of Transcription by a Tissue-Specific TAF Homolog.” *Genes & Development* 15 (8): 1021–30.

Hiller, Mark, Xin Chen, M. Jodeane Pringle, Martin Suchorolski, Yasemin Sancak, Sridhar Viswanathan, Benjamin Bolival, Ting-Yi Lin, Susan Marino, and Margaret T. Fuller. 2004. “Testis-Specific TAF Homologs Collaborate to Control a Tissue-Specific Transcription Program.” *Development* 131 (21): 5297–5308.

Hinson, S., J. Pettus, and R. N. Nagoshi. 1999. “Regulatory and Functional Interactions between Ovarian Tumor and Ovo during Drosophila Oogenesis.” *Mechanisms of Development* 88 (1): 3–14.

Hubbard, T., D. Barker, E. Birney, G. Cameron, Y. Chen, L. Clark, T. Cox, et al. 2002. “The Ensembl Genome Database Project.” *Nucleic Acids Research* 30 (1): 38–41.

Kent, W. James, Charles W. Sugnet, Terrence S. Furey, Krishna M. Roskin, Tom H. Pringle, Alan M. Zahler, and David Haussler. 2002. “The Human Genome Browser at UCSC.” *Genome Research* 12 (6): 996–1006.

Kim, Daehwan, Joseph M. Paggi, Chanhee Park, Christopher Bennett, and Steven L. Salzberg. 2019. “Graph-Based Genome Alignment and Genotyping with HISAT2 and HISAT-Genotype.” *Nature Biotechnology* 37 (8): 907–15.

Komitopoulou, K., M. Gans, L. H. Margaritis, F. C. Kafatos, and M. Masson. 1983. “Isolation and Characterization of Sex-Linked Female-Sterile Mutants in DROSOPHILA MELANOGASTER with Special Attention to Eggshell Mutants.” *Genetics* 105 (4): 897–920.

Lasko, Paul. 2012. “mRNA Localization and Translational Control in Drosophila Oogenesis.” *Cold Spring Harbor Perspectives in Biology* 4 (10). https://doi.org/10.1101/cshperspect.a012294.

Lee, S., and M. D. Garfinkel. 2000. “Characterization of Drosophila OVO Protein DNA Binding Specificity Using Random DNA Oligomer Selection Suggests Zinc Finger Degeneration.” *Nucleic Acids Research* 28 (3): 826–34.

Li, Jian, and David S. Gilmour. 2013. “Distinct Mechanisms of Transcriptional Pausing Orchestrated by GAGA Factor and M1BP, a Novel Transcription Factor.” *The EMBO Journal* 32 (13): 1829–41.

Lim, Chin Yan, Buyung Santoso, Thomas Boulay, Emily Dong, Uwe Ohler, and James T. Kadonaga. 2004. “The MTE, a New Core Promoter Element for Transcription by RNA Polymerase II.” *Genes & Development* 18 (13): 1606–17.

Li, Victor C., Jerel C. Davis, Kapa Lenkov, Benjamin Bolival, Margaret T. Fuller, and Dmitri A. Petrov. 2009. “Molecular Evolution of the Testis TAFs of Drosophila.” *Molecular Biology and Evolution* 26 (5): 1103–16.

Li, Xiao-Yong, Melissa M. Harrison, Jacqueline E. Villalta, Tommy Kaplan, and Michael B. Eisen. 2014. “Establishment of Regions of Genomic Activity during the Drosophila Maternal to Zygotic Transition.” *eLife* 3 (October): e03737.

Love, Michael I., Wolfgang Huber, and Simon Anders. 2014. “Moderated Estimation of Fold Change and Dispersion for RNA-Seq Data with DESeq2.” *Genome Biology* 15 (12): 550.

Lu, Dan, Ho-Su Sin, Chenggang Lu, and Margaret T. Fuller. 2020. “Developmental Regulation of Cell Type-Specific Transcription by Novel Promoter-Proximal Sequence Elements.” *Genes & Development* 34 (9-10): 663–77.

Lü, J., J. Andrews, D. Pauli, and B. Oliver. 1998. “Drosophila OVO Zinc-Finger Protein Regulates Ovo and Ovarian Tumor Target Promoters.” *Development Genes and Evolution* 208 (4): 213–22.

Lü, J., and B. Oliver. 2001. “Drosophila OVO Regulates Ovarian Tumor Transcription by Binding Unusually near the Transcription Start Site.” *Development* 128 (9): 1671–86.

Mahowald, A. P. 2001. “Assembly of the Drosophila Germ Plasm.” *International Review of Cytology* 203: 187–213.

Mineo, Alessandro, Marc Furriols, and Jordi Casanova. 2017. “Transfer of Dorsoventral and Terminal Information from the Ovary to the Embryo by a Common Group of Eggshell Proteins in Drosophila.” *Genetics* 205 (4): 1529–36.

Nakamura, Shoichi, Seiji Hira, Masato Fujiwara, Nasa Miyagata, Takuma Tsuji, Akane Kondo, Hiroshi Kimura, et al. 2019. “A Truncated Form of a Transcription Factor Mamo Activates Vasa in Drosophila Embryos.” *Communications Biology* 2 (1): 1–13.

Ohler, Uwe, Guo-Chun Liao, Heinrich Niemann, and Gerald M. Rubin. 2002. “Computational Analysis of Core Promoters in the Drosophila Genome.” *Genome Biology* 3 (12): RESEARCH0087.

Oliver, B., D. Pauli, and A. P. Mahowald. 1990. “Genetic Evidence That the Ovo Locus Is Involved in Drosophila Germ Line Sex Determination.” *Genetics* 125 (3): 535–50.

Oliver, B., N. Perrimon, and A. P. Mahowald. 1987. “The Ovo Locus Is Required for Sex-Specific Germ Line Maintenance in Drosophila.” *Genes & Development* 1 (9): 913–23.

Omelina, E. S., E. M. Baricheva, D. Yu Oshchepkov, and T. I. Merkulova. 2011. “Analysis and Recognition of the GAGA Transcription Factor Binding Sites in Drosophila Genes.” *Computational Biology and Chemistry* 35 (6): 363–70.

Pang, Liang-Yu, Steven DeLuca, Haolong Zhu, John M. Urban, and Allan C. Spradling. 2023. “Chromatin and Gene Expression Changes during Female Drosophila Germline Stem Cell Development Illuminate the Biology of Highly Potent Stem Cells.” *eLife* 12 (October): RP90509.

Pauli, D., B. Oliver, and A. P. Mahowald. 1993. “The Role of the Ovarian Tumor Locus in Drosophila Melanogaster Germ Line Sex Determination.” *Development* 119 (1): 123–34.

Quinlan, Aaron R., and Ira M. Hall. 2010. “BEDTools: A Flexible Suite of Utilities for Comparing Genomic Features.” *Bioinformatics* 26 (6): 841–42.

Ramírez, Fidel, Devon P. Ryan, Björn Grüning, Vivek Bhardwaj, Fabian Kilpert, Andreas S. Richter, Steffen Heyne, Friederike Dündar, and Thomas Manke. 2016. “deepTools2: A next Generation Web Server for Deep-Sequencing Data Analysis.” *Nucleic Acids Research* 44 (W1): W160–65.

Raudvere, Uku, Liis Kolberg, Ivan Kuzmin, Tambet Arak, Priit Adler, Hedi Peterson, and Jaak Vilo. 2019. “g:Profiler: A Web Server for Functional Enrichment Analysis and Conversions of Gene Lists (2019 Update).” *Nucleic Acids Research* 47 (W1): W191–98.

R Core Team. 2021. “R: A Language and Environment for Statistical Computing.” *R Foundation for Statistical Computing*. https://www.R-project.org/.

1002 Rice, G. A., M. J. Chamberlin, and C. M. Kane. 1993. “Contacts between Mammalian RNA Polymerase II
1003 and the Template DNA in a Ternary Elongation Complex.” *Nucleic Acids Research* 21 (1): 113–18.
1004 Salles, Cathy, Maryvonne Mével-Ninio, Alain Vincent, and François Payre. 2002. “A Germline-Specific
1005 Splicing Generates an Extended Ovo Protein Isoform Required for Drosophila Oogenesis.”
1006 *Developmental Biology* 246 (2): 366–76.
1007 Santos, Gilberto dos, Andrew J. Schroeder, Joshua L. Goodman, Victor B. Strelets, Madeline A. Crosby,
1008 Jim Thurmond, David B. Emmert, William M. Gelbart, and FlyBase Consortium. 2015. “FlyBase:
1009 Introduction of the Drosophila Melanogaster Release 6 Reference Genome Assembly and Large-
1010 Scale Migration of Genome Annotations.” *Nucleic Acids Research* 43 (Database issue): D690–97.
1011 Smolko, Anne E., Laura Shapiro-Kulnane, and Helen K. Salz. 2018. “The H3K9 Methyltransferase
1012 SETDB1 Maintains Female Identity in Drosophila Germ Cells.” *Nature Communications* 9 (1): 1–11.
1013 Soruco, Marcela M. L., Jessica Chery, Eric P. Bishop, Trevor Siggers, Michael Y. Tolstorukov, Alexander
1014 R. Leydon, Arthur U. Sugden, et al. 2013. “The CLAMP Protein Links the MSL Complex to the X
1015 Chromosome during Drosophila Dosage Compensation.” *Genes & Development* 27 (14): 1551–56.
1016 Spradling, Allan C., Wanbao Niu, Qi Yin, Madhulika Pathak, and Bhawana Maurya. 2022. “Conservation
1017 of Oocyte Development in Germline Cysts from Drosophila to Mouse.” *eLife* 11 (November): e83230.
1018 Ventura, Gemma, Marc Furriols, Nicolás Martín, Vitor Barbosa, and Jordi Casanova. 2010. “Closca, a
1019 New Gene Required for Both Torso RTK Activation and Vitelline Membrane Integrity. Germline
1020 Proteins Contribute to Drosophila Eggshell Composition.” *Developmental Biology* 344 (1): 224–32.
1021 Vo Ngoc, Long, George A. Kassavetis, and James T. Kadonaga. 2019. “The RNA Polymerase II Core
1022 Promoter in Drosophila.” *Genetics* 212 (1): 13–24.
1023 Xu, Zhe, Hongtao Chen, Jia Ling, Danyang Yu, Paolo Struffi, and Stephen Small. 2014. “Impacts of the
1024 Ubiquitous Factor Zelda on Bicoid-Dependent DNA Binding and Transcription in Drosophila.” *Genes
1025 & Development* 28 (6): 608–21.
1026 Zhang, Yong, Tao Liu, Clifford A. Meyer, Jérôme Eeckhoute, David S. Johnson, Bradley E. Bernstein,
1027 Chad Nusbaum, et al. 2008. “Model-Based Analysis of ChIP-Seq (MACS).” *Genome Biology* 9 (9):
1028 R137.
1029

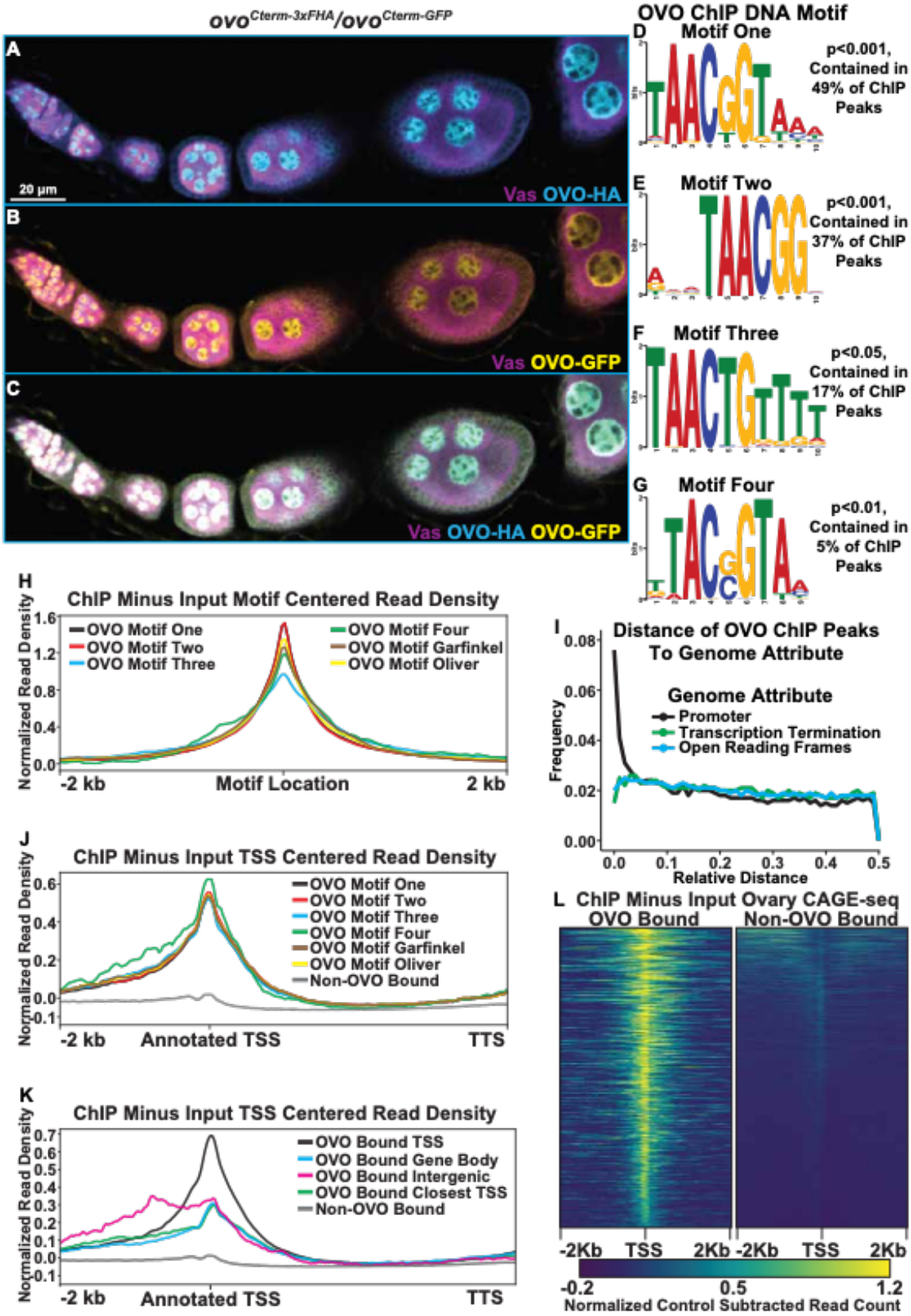
ovo^Cterm-3xFHA/ovo^Cterm-GFP
A
20 µm
Vas OVO-HA
B
Vas OVO-GFP
C
Vas OVO-HA OVO-GFP
OVO ChIP DNA Motif
D Motif One
p<0.001, Contained in 49% of ChIP Peaks
E Motif Two
p<0.001, Contained in 37% of ChIP Peaks
F Motif Three
p<0.05, Contained in 17% of ChIP Peaks
G Motif Four
p<0.01, Contained in 5% of ChIP Peaks
H
ChIP Minus Input Motif Centered Read Density
Normalized Read Density
OVO Motif One
OVO Motif Two
OVO Motif Three
OVO Motif Four
OVO Motif Garfinkel
OVO Motif Oliver
-2 kb
Motif Location
2 kb
I
Distance of OVO ChIP Peaks To Genome Attribute
Genome Attribute
Promoter
Transcription Termination
Open Reading Frames
Frequency
Relative Distance
J
ChIP Minus Input TSS Centered Read Density
Normalized Read Density
OVO Motif One
OVO Motif Two
OVO Motif Three
OVO Motif Four
OVO Motif Garfinkel
OVO Motif Oliver
Non-OVO Bound
-2 kb
Annotated TSS
TTS
K
ChIP Minus Input TSS Centered Read Density
Normalized Read Density
OVO Bound TSS
OVO Bound Gene Body
OVO Bound Intergenic
OVO Bound Closest TSS
Non-OVO Bound
-2 kb
Annotated TSS
TTS
L ChIP Minus Input Ovary CAGE-seq
OVO Bound
Non-OVO Bound
-2Kb TSS 2Kb -2Kb TSS 2Kb
-0.2 0.5 1.2
Normalized Control Subtracted Read Count

1030

1031 **Figure 1: Significantly Enriched OVO DNA Binding Motifs and OVO ChIP Attributes Genome-Wide.**
1032 A-C) Immunofluorescent staining of adult ovarioles of *ovo*$^{Cterm\text{-}3xFHA}$/*ovo*$^{Cterm\text{-}GFP}$ females (20x, scale bar =
1033 20 µm). Ovarioles were stained for Vas (purple) to label the germline, HA (cyan) to label OVO-HA, and
1034 GFP (yellow) to label OVO-GFP. The homozygous version of these alleles were used to ChIP OVO. D-G)
1035 Significantly enriched motifs found within overlapping OVO ChIP peaks. The percentage of OVO ChIP
1036 peaks containing each motif and their corresponding p-value are indicated to the right. H) OVO ChIP
1037 minus input control ChIP-seq read coverage density centered on the location of the four *de novo* OVO
1038 DNA binding motifs and previously defined *in vitro* OVO DNA binding motifs (Lü et al. 1998, Bielinska et
1039 al. 2005, Lee and Garfinkel 2000). I) Relative distance of OVO ChIP peaks to gene level promoters,
1040 terminations sequences, and open reading frames genome-wide. J) OVO ChIP minus input control ChIP-
1041 seq read coverage density for genes containing significant OVO ChIP peaks and the corresponding OVO
1042 DNA binding motif. Genes are centered on the transcriptional start site. K) OVO ChIP minus input control
1043 ChIP-seq read coverage density for genes bound by OVO over the TSS, gene body, closest TSS in
1044 intergenic space, closest TSS for all, or not bound. Genes are centered on the transcriptional start site. L)
1045 OVO ChIP minus input control ChIP-seq heatmaps centered on the dominant significant ovary CAGE-seq
1046 TSSs overlapping or not overlapping OVO ChIP peaks.

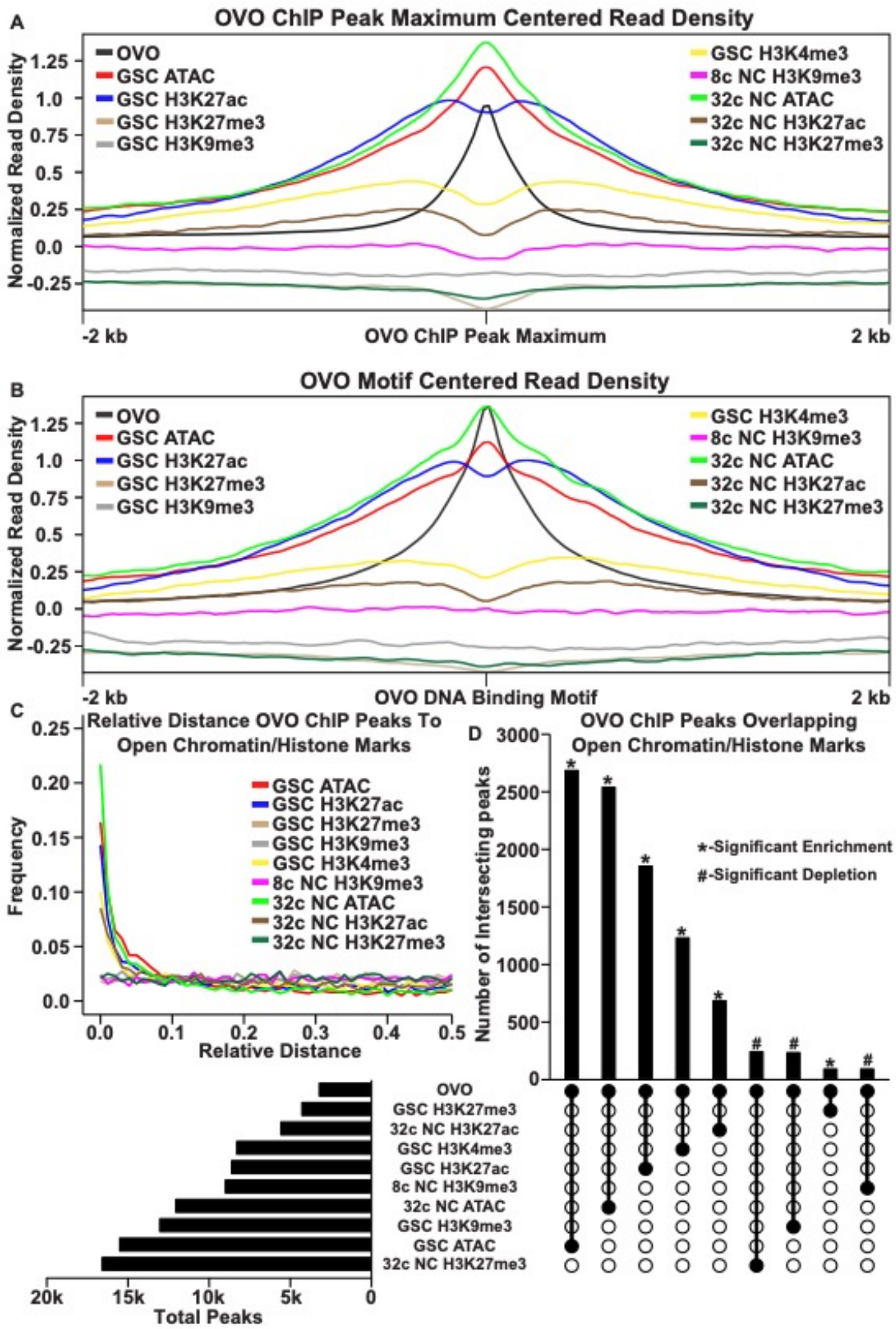
A
OVO ChIP Peak Maximum Centered Read Density
Normalized Read Density
OVO
GSC ATAC
GSC H3K27ac
GSC H3K27me3
GSC H3K9me3
GSC H3K4me3
8c NC H3K9me3
32c NC ATAC
32c NC H3K27ac
32c NC H3K27me3
-2 kb
OVO ChIP Peak Maximum
2 kb
B
OVO Motif Centered Read Density
OVO DNA Binding Motif
C
Relative Distance OVO ChIP Peaks To Open Chromatin/Histone Marks
Frequency
Relative Distance
D
OVO ChIP Peaks Overlapping Open Chromatin/Histone Marks
Number of Intersecting peaks
*-Significant Enrichment
#-Significant Depletion
Total Peaks

1047

1048 **Figure 2: OVO DNA Binding is Associated with Open Chromatin and Transcriptionally Active**
1049 **Histone Marks.** A, B) OVO ChIP minus input control, GSC and 32c ATAC-seq, GSC H3K27ac,
1050 H3K4me3, H3K27me3, H3K9me3, 8c NC H3K9me3, 32c NC H3K27ac, and H3K27me3 ChIP-seq read
1051 coverage density centered on each OVO peak maximum or OVO DNA binding motif located within a
1052 significant OVO ChIP peak. C) Relative distance of OVO ChIP peaks to significantly called peaks for GSC
1053 and 32c ATAC-seq, GSC H3K27ac, H3K4me3, H3K27me3, H3K9me3, 8c NC H3K9me3, 32c NC
1054 H3K27ac, and H3K27me3 ChIP-seq genome-wide. D) Total number of significant peaks (left) and the
1055 total number of overlapping peaks (top) between OVO ChIP and GSC and 32c ATAC-seq, GSC
1056 H3K27ac, H3K4me3, H3K27me3, H3K9me3, 8c NC H3K9me3, 32c NC H3K27ac, and H3K27me3 ChIP-
1057 seq. Lines connecting solid dots indicates the amount of overlapping peaks between those two
1058 corresponding datasets. Asterisk indicates significantly enriched overlap while hashtag indicates
1059 significantly depleted overlap between datasets.

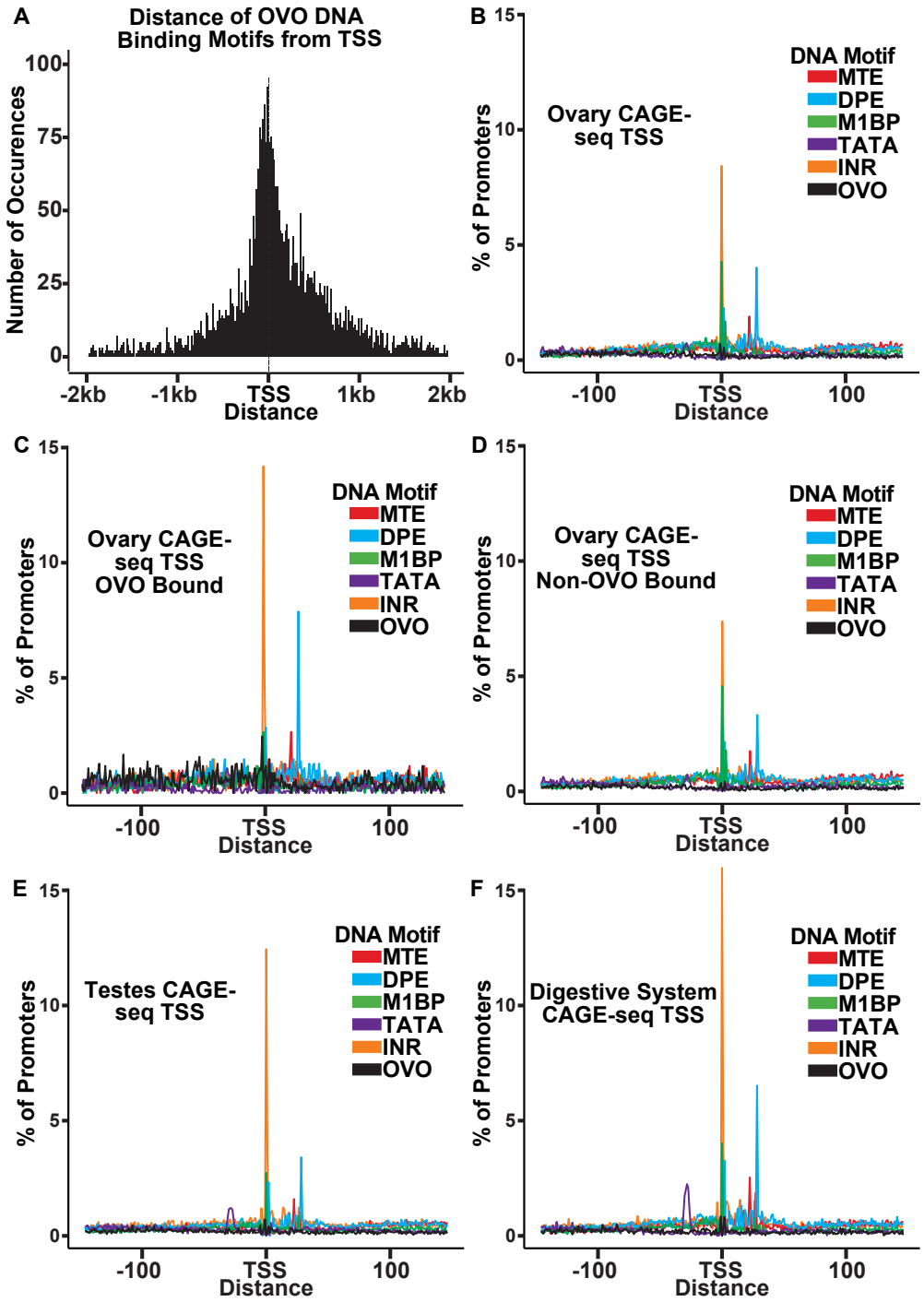
A
Distance of OVO DNA Binding Motifs from TSS
Number of Occurences
100
75
50
25
0
-2kb
-1kb
TSS
1kb
2kb
Distance
B
Ovary CAGE-seq TSS
% of Promoters
DNA Motif
MTE
DPE
M1BP
TATA
INR
OVO
-100
TSS
100
Distance
C
Ovary CAGE-seq TSS OVO Bound
D
Ovary CAGE-seq TSS Non-OVO Bound
E
Testes CAGE-seq TSS
F
Digestive System CAGE-seq TSS

1060

1061 **Figure 3: OVO Bound Promoters are Enriched for INR, DPE, and MTE elements.** A) Histogram of the
1062 distance of *in vivo* and *in vitro* OVO DNA binding motifs within significant overlapping OVO ChIP peaks
1063 from the closest genes TSS. B-F) Histogram of the percent of promoters from tissue specific CAGE-seq
1064 analysis of common promoter motif elements centered on the dominant significant TSS.

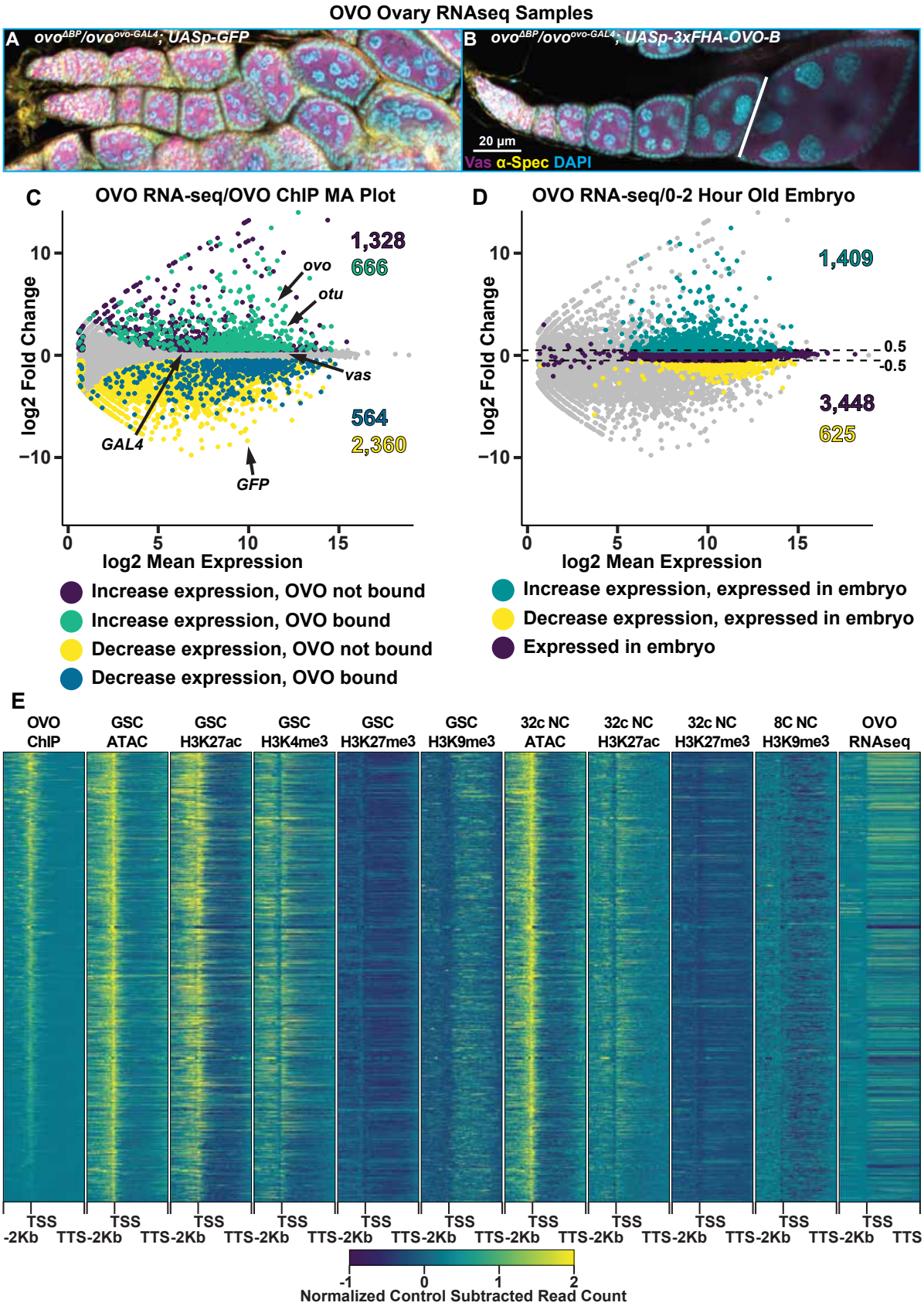
OVO Ovary RNAseq Samples
A ovoΔBP/ovoovo-GAL4; UASp-GFP
B ovoΔBP/ovoovo-GAL4; UASp-3xFHA-OVO-B
20 µm
Vas α-Spec DAPI
C
OVO RNA-seq/OVO ChIP MA Plot
1,328
666
ovo
otu
vas
564
2,360
GAL4
GFP
log2 Fold Change
log2 Mean Expression
Increase expression, OVO not bound
Increase expression, OVO bound
Decrease expression, OVO not bound
Decrease expression, OVO bound
D
OVO RNA-seq/0-2 Hour Old Embryo
1,409
0.5
-0.5
3,448
625
log2 Fold Change
log2 Mean Expression
Increase expression, expressed in embryo
Decrease expression, expressed in embryo
Expressed in embryo
E
OVO ChIP
GSC ATAC
GSC H3K27ac
GSC H3K4me3
GSC H3K27me3
GSC H3K9me3
32c NC ATAC
32c NC H3K27ac
32c NC H3K27me3
8C NC H3K9me3
OVO RNAseq
TSS -2Kb
TSS TTS-2Kb
TTS
Normalized Control Subtracted Read Count

1065

1066 **Figure 4: Genes Bound by OVO Increase in Expression in the Presence of OVO Genome-Wide.** A-
1067 B) Immunofluorescent staining of adult ovarioles of the indicated genotypes (20x, scale bar = 20 μm).
1068 Ovarioles were stained for Vas (purple) to label the germline, α-Spectrin (yellow) to label dot spectrosome
1069 and fusomes, and DAPI (cyan) to label nuclei. Line indicates the dissection point for germarium through
1070 previtellogenic RNA-seq samples. C) MA plot of *ovo*$^{\Delta BP}$/*ovo*$^{ovo\text{-}GAL4}$; *UASp-3xFHA-OVO-B* versus
1071 *ovo*$^{\Delta BP}$/*ovo*$^{ovo\text{-}GAL4}$; *UASp-GFP* RNA-seq differential expression results. Purple dots indicate genes that
1072 significantly increased in expression and were not bound by OVO, cyan dots indicate genes that
1073 significantly increased in expression and were bound by OVO, yellow dots indicate genes that
1074 significantly decreased in gene expression and were not bound by OVO, blue dots indicate genes that
1075 significantly decreased in gene expression and were bound by OVO, and gray dots indicate genes that
1076 were not differentially expressed from our analysis. D) MA plot of *ovo*$^{\Delta BP}$/*ovo*$^{ovo\text{-}GAL4}$; *UASp-3xFHA-OVO-B*
1077 versus *ovo*$^{\Delta BP}$/*ovo*$^{ovo\text{-}GAL4}$; *UASp-GFP* RNA-seq differential expression results. Cyan dots indicate genes
1078 that significantly increased in expression and were found to be moderately expressed in 0-2 hour old
1079 embryos, yellow dots indicate genes that significantly decreased in gene expression and were found to be
1080 moderately expressed in 0-2 hour old embryos, purple dots indicate genes that were not differentially
1081 expressed and were found to be moderately expressed in 0-2 hour old embryos, and gray dots indicate
1082 genes that were not differentially expressed and were not found to be moderately expressed in 0-2 hour
1083 old embryos. E) Gene level read coverage heatmaps of OVO ChIP minus input, GSC and 32c ATAC-seq,
1084 GSC H3K27ac, H3K4me3, H3K27me3, H3K9me3, 8c NC H3K9me3, 32c NC H3K27ac, and H3K27me3
1085 ChIP-seq, and *ovo*$^{\Delta BP}$/*ovo*$^{ovo\text{-}GAL4}$; *UASp-3xFHA-OVO-B* minus *ovo*$^{\Delta BP}$/*ovo*$^{ovo\text{-}GAL4}$; *UASp-GFP* RNA-seq
1086 for genes bound by OVO. The order of the heatmap is genes with the highest to lowest amount of OVO
1087 ChIP read density.

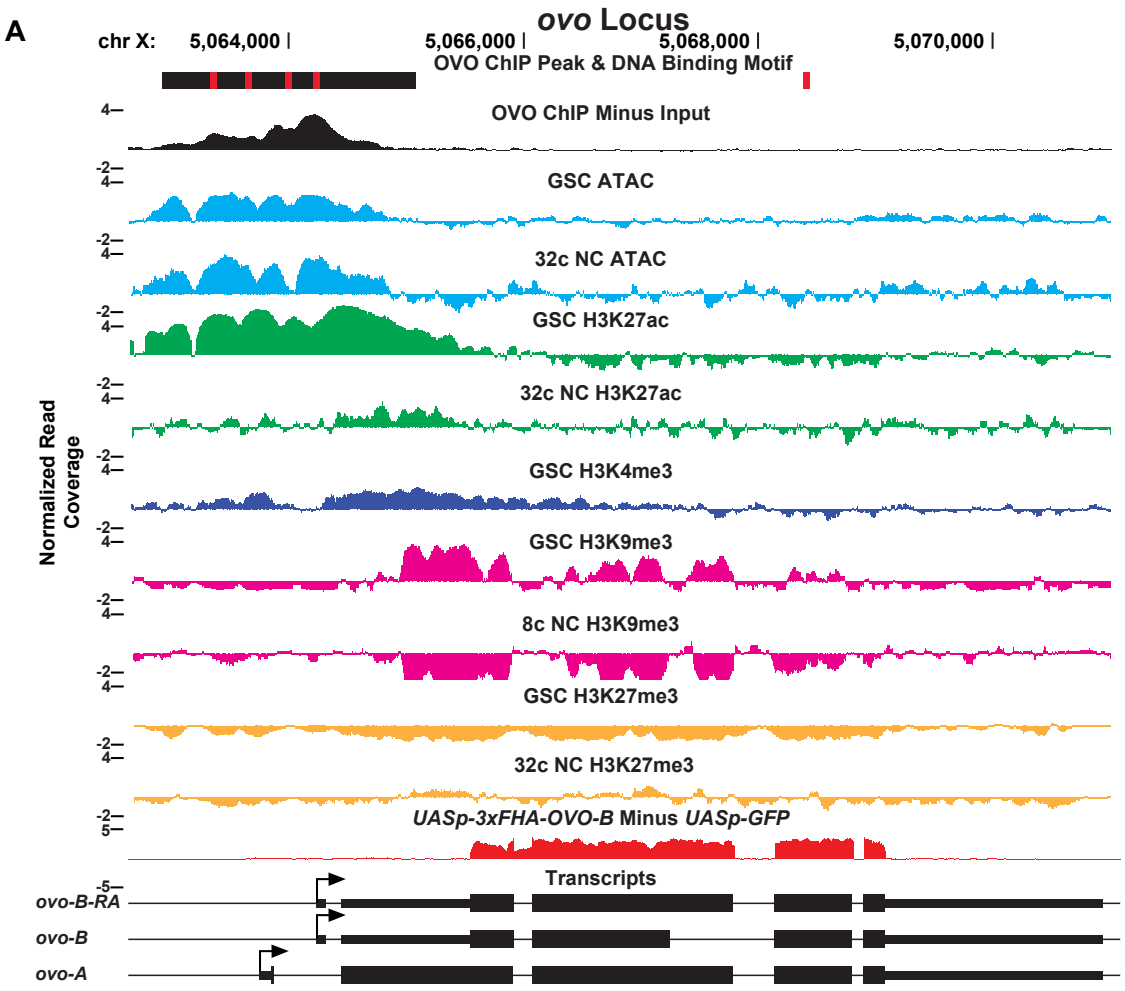
A
ovo Locus
chr X:
5,064,000
5,066,000
5,068,000
5,070,000
OVO ChIP Peak & DNA Binding Motif
OVO ChIP Minus Input
GSC ATAC
32c NC ATAC
GSC H3K27ac
32c NC H3K27ac
GSC H3K4me3
GSC H3K9me3
8c NC H3K9me3
GSC H3K27me3
32c NC H3K27me3
UASp-3xFHA-OVO-B Minus UASp-GFP
Normalized Read Coverage
Transcripts
ovo-B-RA
ovo-B
ovo-A

1088

1089 **Figure 5: OVO ChIP-seq, ATAC/Histone ChIP-seq, RNA-seq, and DNA Binding Motifs at the *ovo***
1090 **Locus.** *ovo* gene level read coverage tracks for OVO ChIP minus input (black), GSC and 32c ATAC-seq
1091 (light blue), GSC and 32C H3K27ac (green), H3K4me3 (dark blue), GSC and 32c H3K27me3 (orange),
1092 and GSC and 8c H3K9me3 (pink) ChIP-seq, and $ovo^{\Delta BP}/ovo^{ovo\text{-}GAL4}$; *UASp-3xFHA-OVO-B* minus
1093 $ovo^{\Delta BP}/ovo^{ovo\text{-}GAL4}$; *UASp-GFP* RNA-seq (red). Red rectangles and black rectangles represent significant
1094 OVO DNA binding motifs and OVO ChIP peaks, respectively. Gene models are represented at bottom.
1095 Small rectangles represent untranslated regions, large rectangles represent translated regions. Arrows
1096 indicate transcriptional start sites.

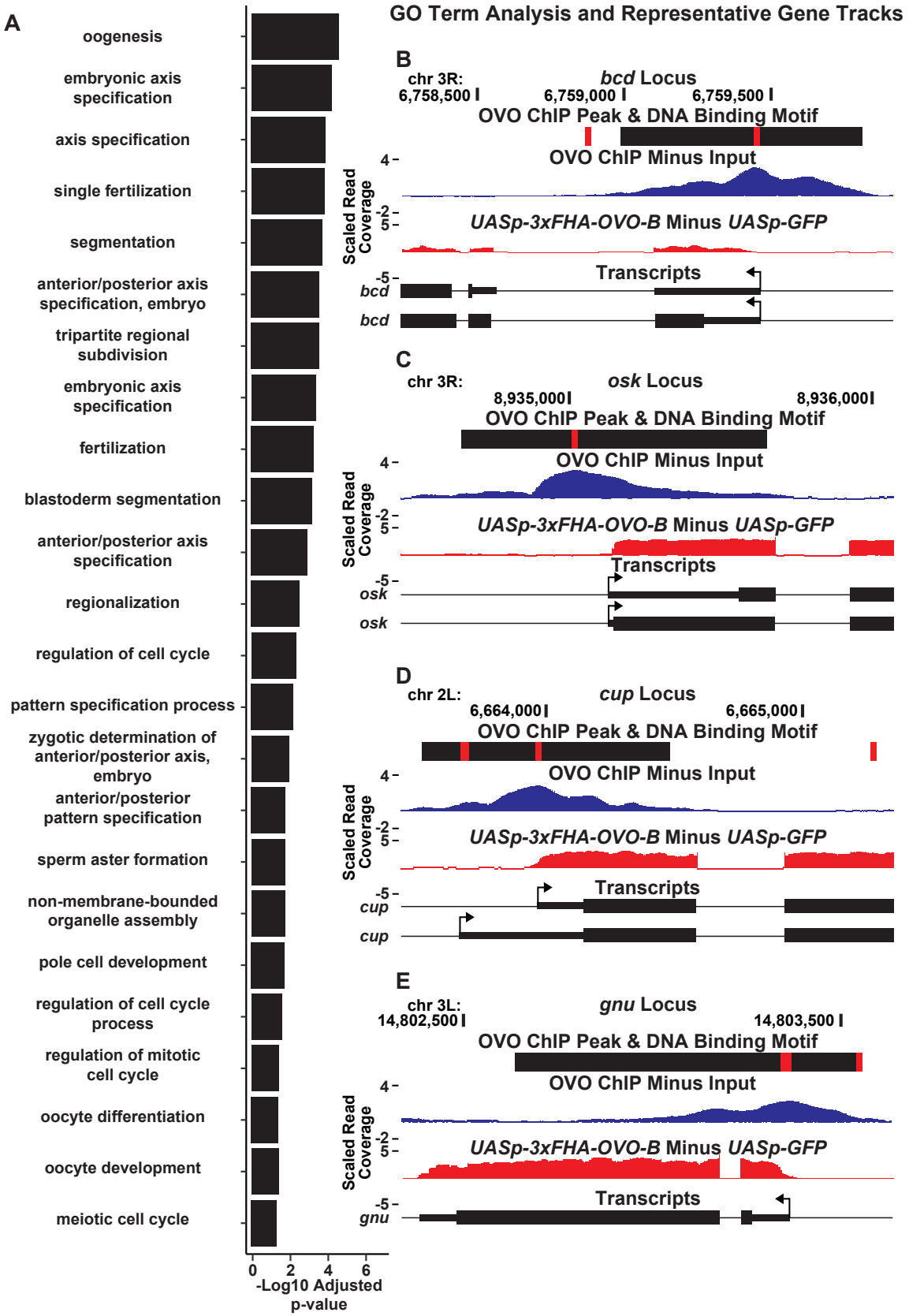
A
oogenesis
embryonic axis specification
axis specification
single fertilization
segmentation
anterior/posterior axis specification, embryo
tripartite regional subdivision
embryonic axis specification
fertilization
blastoderm segmentation
anterior/posterior axis specification
regionalization
regulation of cell cycle
pattern specification process
zygotic determination of anterior/posterior axis, embryo
anterior/posterior pattern specification
sperm aster formation
non-membrane-bounded organelle assembly
pole cell development
regulation of cell cycle process
regulation of mitotic cell cycle
oocyte differentiation
oocyte development
meiotic cell cycle
0 2 4 6
-Log10 Adjusted p-value
GO Term Analysis and Representative Gene Tracks
B
chr 3R:
bcd Locus
6,758,500
6,759,000
6,759,500
OVO ChIP Peak & DNA Binding Motif
OVO ChIP Minus Input
UASp-3xFHA-OVO-B Minus UASp-GFP
Scaled Read Coverage
Transcripts
bcd
bcd
C
chr 3R:
osk Locus
8,935,000
8,936,000
OVO ChIP Peak & DNA Binding Motif
OVO ChIP Minus Input
UASp-3xFHA-OVO-B Minus UASp-GFP
Scaled Read Coverage
Transcripts
osk
osk
D
chr 2L:
cup Locus
6,664,000
6,665,000
OVO ChIP Peak & DNA Binding Motif
OVO ChIP Minus Input
UASp-3xFHA-OVO-B Minus UASp-GFP
Scaled Read Coverage
Transcripts
cup
cup
E
chr 3L:
gnu Locus
14,802,500
14,803,500
OVO ChIP Peak & DNA Binding Motif
OVO ChIP Minus Input
UASp-3xFHA-OVO-B Minus UASp-GFP
Scaled Read Coverage
Transcripts
gnu

1097

1098 **Figure 6: OVO Binds and Significantly Increases the Expression of a Number of Genes Involved in**
1099 **Essential Maternal Processes.** A) Significantly enriched GO biological process terms for genes bound
1100 by OVO and significantly increase in expression in the presence of ectopic rescue OVO. GO terms are
1101 restricted to the 24 smallest term sizes. B-E) Example GO term gene level read coverage tracks for OVO
1102 ChIP minus input and $ovo^{\Delta BP}/ovo^{ovo\text{-}GAL4}$; *UASp-3xFHA-OVO-B* minus $ovo^{\Delta BP}/ovo^{ovo\text{-}GAL4}$; *UASp-GFP*. Red
1103 rectangles and black rectangles represent significant OVO DNA binding motifs and OVO ChIP peaks,
1104 respectively. Gene models are represented at bottom. Small rectangles represent untranslated regions,
1105 large rectangles represent translated regions. Arrows indicate transcriptional start sites.
1106
1107 **Table S1: OVO ChIP-seq Results by Chromosome.**
1108 **Table S2: Genomic Locations of Significant Overlapping OVO ChIP Peaks**
1109 **Table S3: Significant OVO DNA Binding Motifs in MEME Format**
1110 **Table S4: Differential Expression Analysis Results for All Genes**
1111 **Table S5: Significantly Enriched GO Biological Process Terms**
1112 **Table S6: Flybase ART Table.**

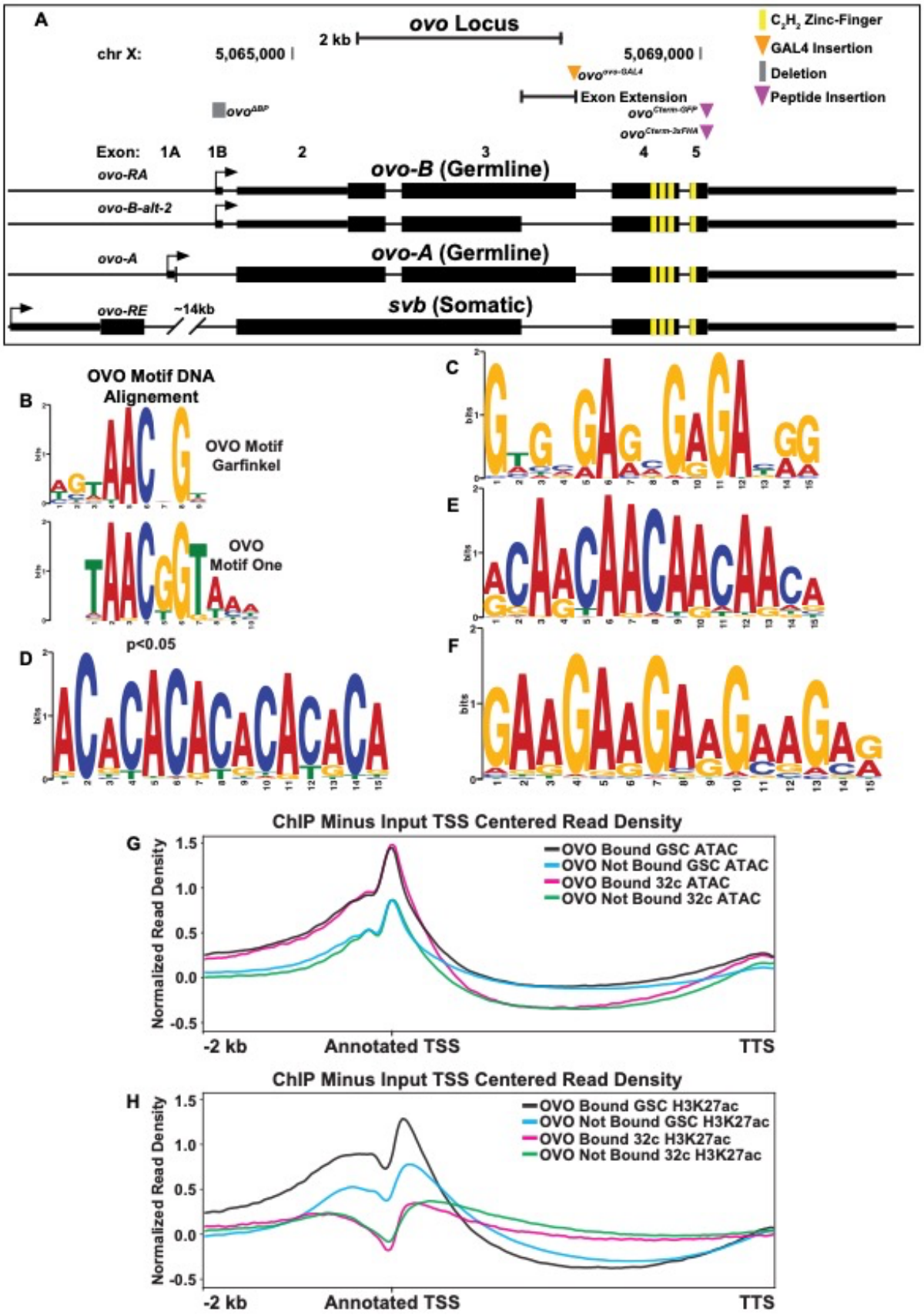
A
ovo Locus
2 kb
chr X:
5,065,000
5,069,000
C2H2 Zinc-Finger
GAL4 Insertion
Deletion
Peptide Insertion
Exon Extension
Exon: 1A 1B 2 3 4 5
ovo-RA
ovo-B (Germline)
ovo-B-alt-2
ovo-A
ovo-A (Germline)
ovo-RE
~14kb
svb (Somatic)
B
OVO Motif DNA Alignement
OVO Motif Garfinkel
OVO Motif One
C
D
p<0.05
E
F
G
ChIP Minus Input TSS Centered Read Density
Normalized Read Density
OVO Bound GSC ATAC
OVO Not Bound GSC ATAC
OVO Bound 32c ATAC
OVO Not Bound 32c ATAC
-2 kb
Annotated TSS
TTS
H
ChIP Minus Input TSS Centered Read Density
Normalized Read Density
OVO Bound GSC H3K27ac
OVO Not Bound GSC H3K27ac
OVO Bound 32c H3K27ac
OVO Not Bound 32c H3K27ac
-2 kb
Annotated TSS
TTS

1113

1114 **Figure S1: Significant OVO DNA Binding Motif.** A) Cartoon of the transcripts expressed from the *ovo*
1115 locus based on Benner et al. 2023. Gray box represents endogenously generated deletions, orange
1116 triangle represents the location of the *T2A-GAL4-3xSTOP* insertion, purple triangles represent the
1117 location of small peptide insertions and yellow boxes represent the location of the shared C_2H_2 zinc-
1118 fingers. Small rectangles represent untranslated regions, large rectangles represent translated regions
1119 and arrows indicate TSSs. B) Significant alignment of the *in vivo* OVO DNA binding 'motif one' and *in vitro*
1120 OVO DNA binding motif (Lee and Garfinkel 2000). C-F) Significantly enriched DNA motifs within OVO
1121 ChIP peaks. C is a signficiant match for the DNA binding motif of GAF and CLAMP (Omelina et al. 2011;
1122 Soruco et al. 2013). G, H. GSC and 32c ATAC-seq and H3K27ac ChIP-seq minus input control read
1123 coverage density for genes bound by OVO over the TSS, gene body, closest TSS in intergenic space,
1124 closest TSS for all, or not bound. Plots are centered on the TSS.

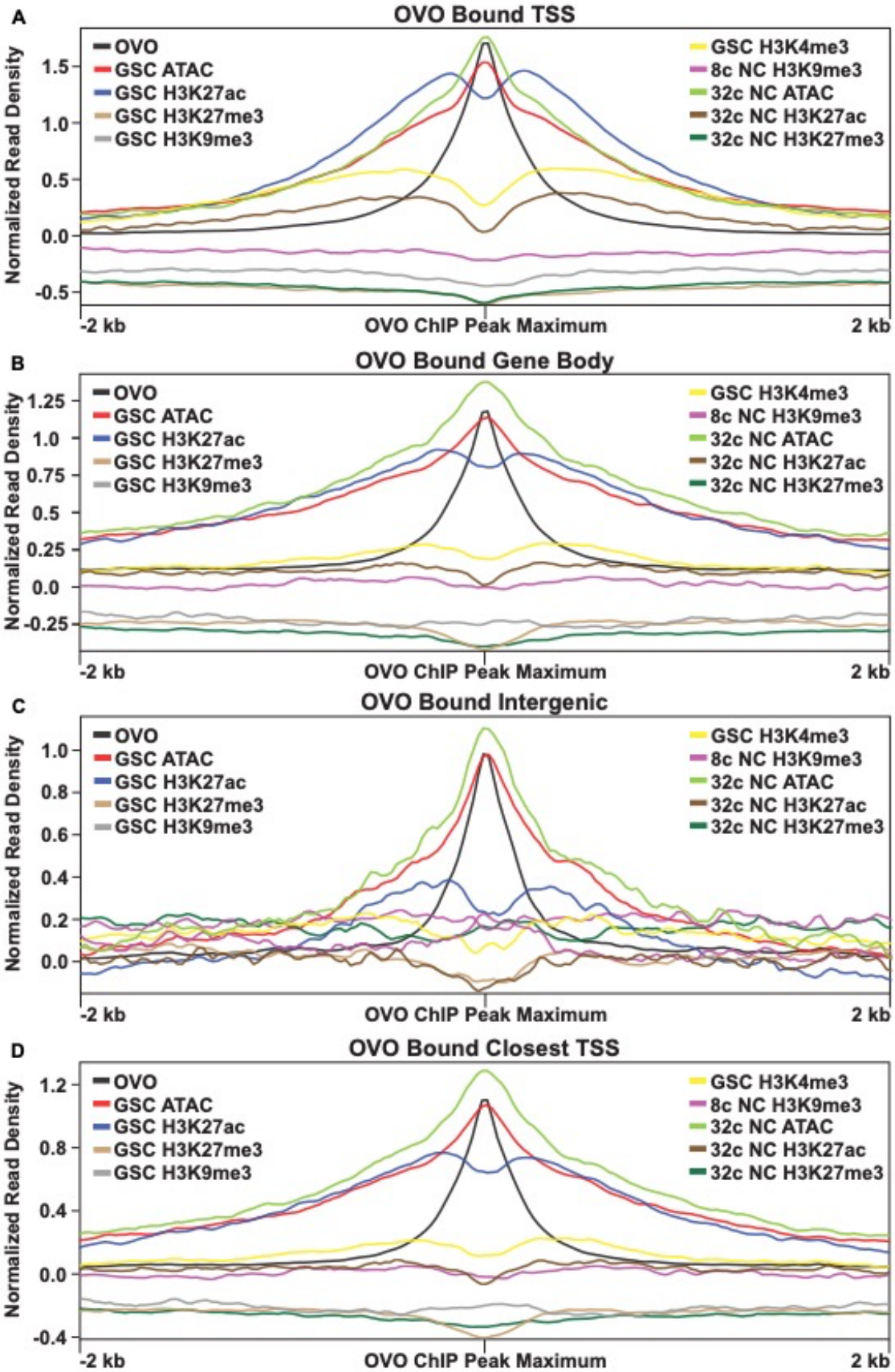
A
OVO Bound TSS
Normalized Read Density
1.5
1.0
0.5
0.0
-0.5
OVO
GSC ATAC
GSC H3K27ac
GSC H3K27me3
GSC H3K9me3
GSC H3K4me3
8c NC H3K9me3
32c NC ATAC
32c NC H3K27ac
32c NC H3K27me3
-2 kb
OVO ChIP Peak Maximum
2 kb
B
OVO Bound Gene Body
Normalized Read Density
1.25
1.0
0.75
0.5
0.25
0.0
-0.25
OVO
GSC ATAC
GSC H3K27ac
GSC H3K27me3
GSC H3K9me3
GSC H3K4me3
8c NC H3K9me3
32c NC ATAC
32c NC H3K27ac
32c NC H3K27me3
-2 kb
OVO ChIP Peak Maximum
2 kb
C
OVO Bound Intergenic
Normalized Read Density
1.0
0.8
0.6
0.4
0.2
0.0
OVO
GSC ATAC
GSC H3K27ac
GSC H3K27me3
GSC H3K9me3
GSC H3K4me3
8c NC H3K9me3
32c NC ATAC
32c NC H3K27ac
32c NC H3K27me3
-2 kb
OVO ChIP Peak Maximum
2 kb
D
OVO Bound Closest TSS
Normalized Read Density
1.2
0.8
0.4
0.0
-0.4
OVO
GSC ATAC
GSC H3K27ac
GSC H3K27me3
GSC H3K9me3
GSC H3K4me3
8c NC H3K9me3
32c NC ATAC
32c NC H3K27ac
32c NC H3K27me3
-2 kb
OVO ChIP Peak Maximum
2 kb

1125

1126 **Figure S2: OVO DNA Binding is Associated with Open Chromatin and Transcriptionally Active**
1127 **Histone Marks Across Variations of Gene Binding Patterns.** A-D) OVO ChIP minus input control,
1128 GSC and 32c ATAC-seq, GSC H3K27ac, H3K4me3, H3K27me3, H3K9me3, 8c NC H3K9me3, 32c NC
1129 H3K27ac, and H3K27me3 ChIP-seq read coverage density centered on OVO peak maximums located
1130 within a significant OVO ChIP peak for genes bound by OVO over the TSS, gene body, closest TSS in
1131 intergenic space, or closest TSS for all.

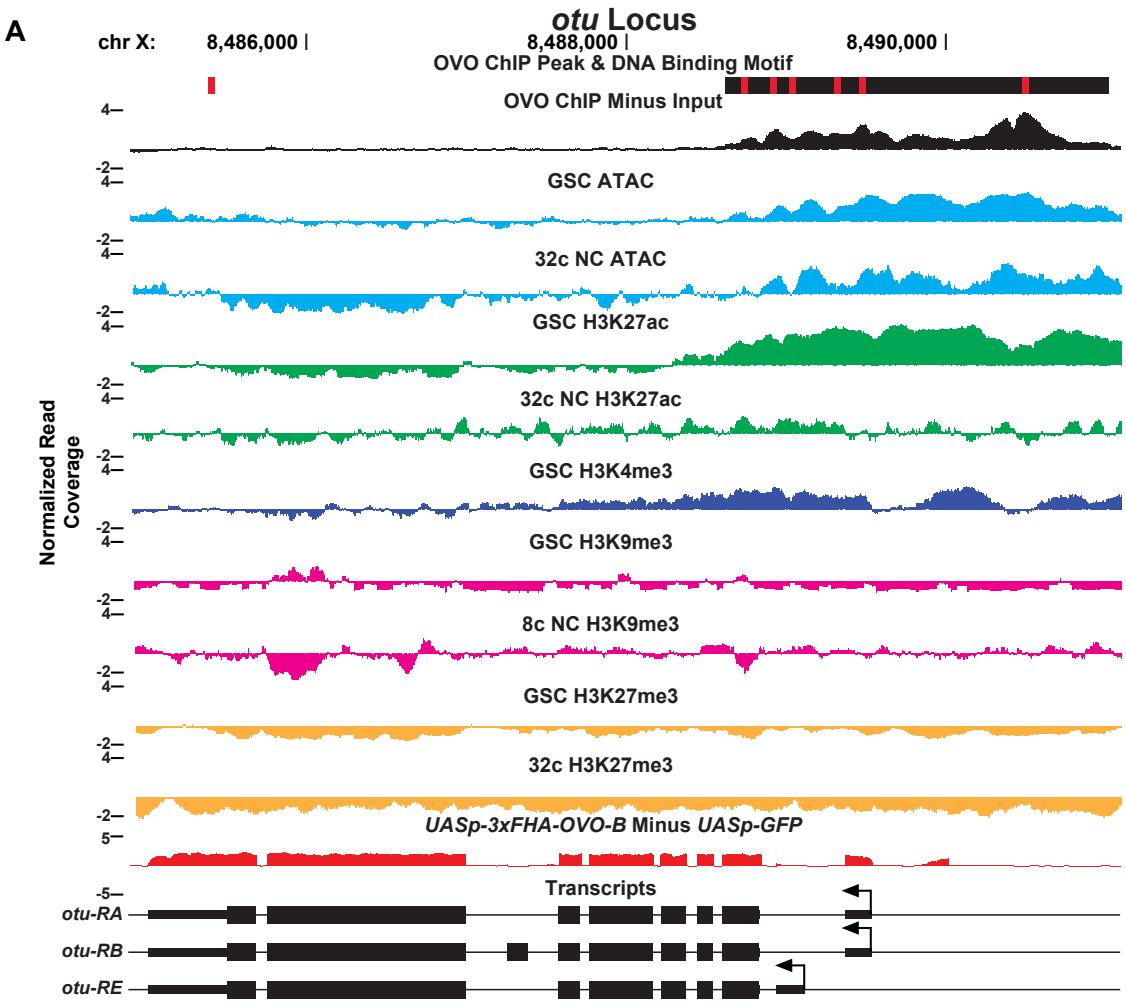
A
otu Locus
chr X:
8,486,000
8,488,000
8,490,000
OVO ChIP Peak & DNA Binding Motif
OVO ChIP Minus Input
GSC ATAC
32c NC ATAC
GSC H3K27ac
32c NC H3K27ac
GSC H3K4me3
GSC H3K9me3
8c NC H3K9me3
GSC H3K27me3
32c H3K27me3
UASp-3xFHA-OVO-B Minus UASp-GFP
Normalized Read Coverage
Transcripts
otu-RA
otu-RB
otu-RE

1132

1133 **Figure S3: OVO ChIP-seq, ATAC/Histone ChIP-seq, RNA-seq, and DNA Binding Motifs at the *otu***
1134 **Locus.** A) *otu* gene level read coverage tracks for OVO ChIP minus input (black), GSC and 32c ATAC-
1135 seq (light blue), GSC and 32C H3K27ac (green), H3K4me3 (dark blue), GSC and 32c H3K27me3
1136 (orange), and GSC and 8c H3K9me3 (pink) ChIP-seq, and $ovo^{\Delta BP}/ovo^{ovo\text{-}GAL4}$; *UASp-3xFHA-OVO-B*
1137 minus $ovo^{\Delta BP}/ovo^{ovo\text{-}GAL4}$; *UASp-GFP* RNA-seq (red). Red rectangles and black rectangles represent
1138 significant OVO DNA binding motifs and OVO ChIP peaks, respectively. Gene models are represented at
1139 bottom. Small rectangles represent untranslated regions, large rectangles represent translated regions.
1140 Arrows indicate transcriptional start sites.